Studying the Interplay Between the Actor and Critic Representations in Reinforcement Learning

Samuel Garcin[*]
University of Edinburgh

Trevor McInroe[*]
University of Edinburgh

Pablo Samuel Castro
Google DeepMind, Mila

Prakash Panangaden
McGill, Mila

Christopher G. Lucas
University of Edinburgh

David Abel
Google DeepMind, University of Edinburgh

Stefano V. Albrecht
University of Edinburgh

Abstract

Extracting relevant information from a stream of high-dimensional observations is a central challenge for deep reinforcement learning agents. Actor-critic algorithms add further complexity to this challenge, as it is often unclear whether the same information will be relevant to both the actor and the critic. To this end, we here explore the principles that underlie effective representations for the actor and for the critic in on-policy algorithms. We focus our study on understanding whether the actor and critic will benefit from separate, rather than shared, representations. Our primary finding is that when separated, the representations for the actor and critic systematically specialise in extracting different types of information from the environment—the actor's representation tends to focus on action-relevant information, while the critic's representation specialises in encoding value and dynamics information. We conduct a rigourous empirical study to understand how different representation learning approaches affect the actor and critic's specialisations and their downstream performance, in terms of sample efficiency and generation capabilities. Finally, we discover that a separated critic plays an important role in exploration and data collection during training. Our code, trained models and data are accessible at `https://github.com/francelico/deac-rep`.

1 Introduction

In recent years, auxiliary representation learning objectives have become increasingly prominent in deep reinforcement learning (RL) agents (Yarats et al., 2021a; Dunion et al., 2023a). These objectives facilitate extracting relevant features from high dimensional observations, and can help improve the sample efficiency and generalisation capabilities of both value-based (Anand et al., 2019; Schwarzer et al., 2021) and actor-critic methods (Yarats et al., 2021b; Zhang et al., 2021; McInroe et al., 2023). However, knowing whether a particular representation learning objective will work and understanding *why* it works is often difficult due to the interplay between the different components of modern RL algorithms.

Figure 1: Models with shared (left) and decoupled representations (right).

Online actor-critic algorithms like PPO (Schulman et al., 2017) jointly optimise policy improvement and value estimation objectives. When parametrised by deep neural networks, the actor (in charge of improving the policy) and the critic (in charge of estimating the value of the current policy) often share the same learned representation ϕ, which maps observations to latent features z.
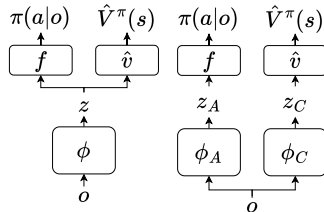
---

[*]Equal contribution. Correspondence to {`s.garcin,t.mcinroe`}`@ed.ac.uk`

Cobbe et al. (2021) and Raileanu & Fergus (2021) report that fully separating the actor and critic networks, i.e. *decoupling* the two (Figure 1, right), improves sample efficiency and generalisation over a shared architecture (Figure 1, left). We hypothesise that decoupling is effective because it encourages information specialisation in ϕ_A and ϕ_C, which in turn improves performance. To test our hypothesis, we introduce metrics to quantify specialisation, and we conduct an extensive empirical study of three on-policy actor-critic algorithms (Schulman et al., 2017; Cobbe et al., 2021; Moon et al., 2022) across discrete and continuous control benchmarks, and under various representation learning approaches (Raileanu & Fergus, 2021; Moon et al., 2022; Raileanu et al., 2021; Castro et al., 2021) applied to the actor, to the critic, or to both. We supplement this empirical study by a theoretical characterisation of the information extracted by the actor and critic's respective optimal representations.

Table 1: Once decoupled, the actor and critic representations ϕ_A and ϕ_C specialise in capturing different information from the environment. Reported values correspond to a PPO agent trained in Procgen (Cobbe et al., 2020). See §2 and §3 for formal definitions of the quantities quoted.

If ... is high,	it is possible to ...	% change from using a shared representation	
		ϕ_A	ϕ_C
$I(Z; L)$	overfit to training levels (environment instances).	-20%	+35%
$I(Z; V)$	use z to predict state values.	+37%	+41%
$I((Z, Z'); A)$	use z and z' obtained from consecutive timesteps t, t' to identify the action taken at timestep t.	+23%	-48%
$I(Z; Z')$	differentiate between latent pairs obtained from consecutive and non-consecutive timesteps.	-96%	+324%

Our main findings are summarised below.

- Decoupled actor and critic representations extract different information about the environment. This information specialisation, described and quantified in Table 1, systematically occurs in the on-policy algorithms and benchmarks covered by our study, and is consistent with the actor's and critic's respective optimal representations.

- The actor benefits from representation learning approaches that prioritise extracting level-invariant information over level-specific information. This bias for level-invariant information matters more than what specific information quantity is targeted by the representation learning objective. Nevertheless, approaches antithetical to the actor's inherent information specialisation tend to perform poorly.

- Through its role as a baseline in the actor's objective, a decoupled critic will tend to bias policy updates to facilitate the optimisation of its own learning objective. The critic, therefore, plays an important role in exploration and data collection during training. Thus, we find that care must be taken when selecting a representation learning objective for the critic: certain objectives improve the critic's value predictions but may prevent convergence to the optimal policy because the objective induces significant bias.

---

2 BACKGROUND

RL framework. We follow the framework established by Kirk et al. (2023), which, given a fixed timestep budget, lets us quantify the agent's performance in its original training environment (i.e. its sample efficiency) and its performance in held-out instances (i.e. its generalisation capabilities). We consider the episodic setting, and model the environment as a Contextual-MDP (CMDP) $\mathcal{M} \triangleq (\mathbb{S}, \mathbb{A}, \mathbb{O}, \mathcal{T}, \Omega, R, \mathbb{C}, P(c), \mathcal{P}_0, \gamma)$ with state, action and observation spaces $\mathbb{S}, \mathbb{A}$ and $\mathbb{O}$ and discount factor γ. In a CMDP, the reward $R : \mathbb{S} \times \mathbb{C} \times \mathbb{A} \to \mathbb{R}$, and observation functions $\Omega : \mathbb{S} \times \mathbb{C} \to \mathbb{O}$ as well as the transition $\mathcal{T} : \mathbb{S} \times \mathbb{C} \times \mathbb{A} \to \mathscr{P}(\mathbb{S})$, and initial state $\mathcal{P}_0 : \mathbb{C} \to \mathscr{P}(\mathbb{S})$ kernels can change with the *context* $c \in \mathbb{C}$, with $c \sim P(c)$ at the start of each episode. The CMDP is

therefore conceptually equivalent to an MDP with state space $\mathbb{X} : \mathbb{S} \times \mathbb{C}$. Each context c maps one-to-one to a particular environment instance, or *level*, and thus represents the component of the state x that cannot change during the episode. The agent's policy $\pi : \mathbb{O} \to \mathscr{P}(\mathbb{A})$ maps observations to action distributions and induce a value function $V^\pi : \mathbb{X} \to \mathbb{R}$ mapping states to expected future returns $V^\pi(x) = \mathbb{E}_\pi[\sum_t^T \gamma^t r_t]$, where $\{r_t\}_{0:T}$ are possible sequences of rewards obtainable when following policy π from x and until the episode terminates. We define the optimal policy π^* as the policy maximising expected returns $\mathbb{E}_{c \sim P(\mathrm{c}), x_0 \sim \mathcal{P}_0(c)}[V^\pi(x_0)]$. During training, we assume access to a limited set of training levels $L \sim P(\mathrm{c})$. We evaluate sample efficiency by measuring returns over L and generalisation by evaluating on an held-out set $L_{\text{test}} \sim P(\mathrm{c})$.

Actor-critic architectures. On-policy actor-critic models consist of a policy network $\pi_{\boldsymbol{\theta}_A}$ and a value network $\hat{V}_{\boldsymbol{\theta}_C}$, with *actor* parameters $\boldsymbol{\theta}_A$ and *critic* parameters $\boldsymbol{\theta}_C$ (we use $\cdot_A / \cdot_C$ when referring to the actor/critic in this work). When learning from high dimensional observations, such as pixels, a representation $\phi : \mathbb{O} \to \mathbb{Z}$ maps observations to latent features $z \in \mathbb{Z}$. When coupled, the policy and value networks share a representation and split into actor and critic heads f and $\hat{v}$. That is, we have $\pi_{\boldsymbol{\theta}_A} \triangleq f_{\boldsymbol{\omega}} \circ \phi_{\boldsymbol{\eta}}$ and $\hat{V}_{\boldsymbol{\theta}_C} \triangleq \hat{v}_{\boldsymbol{\xi}} \circ \phi_{\boldsymbol{\eta}}$, with $\boldsymbol{\theta}_A \triangleq (\boldsymbol{\omega}, \boldsymbol{\eta})$ and $\boldsymbol{\theta}_C \triangleq (\boldsymbol{\xi}, \boldsymbol{\eta})$. When decoupled, two representation functions ϕ_A, ϕ_C with parameters $(\boldsymbol{\eta}_A, \boldsymbol{\eta}_C)$ are learned.

PPO and PPG. In this work, we investigate the representation properties of PPO (Schulman et al., 2017) and Phasic Policy Gradient (PPG) (Cobbe et al., 2021), two actor-critic algorithms that have been reported to benefit from improved sample efficiency and transfer upon decoupling (Raileanu & Fergus, 2021; Cobbe et al., 2021). In PPO, the actor maximises

$$J_\pi(\boldsymbol{\theta}_A) = \mathbb{E}_B\left[\min(\frac{\pi_{\boldsymbol{\theta}_A}(a_t|o_t)}{\pi_{\boldsymbol{\theta}_{A\,old}}(a_t|o_t)}\hat{A}_t, \text{clip}(\frac{\pi_{\boldsymbol{\theta}_A}(a_t|o_t)}{\pi_{\boldsymbol{\theta}_{A\,old}}(a_t|o_t)}, 1-\epsilon, 1+\epsilon)\hat{A}_t) + \beta_H \mathbf{H}(\pi_{\boldsymbol{\theta}_A}(a_t|o_t))\right], \quad (1)$$

where $\boldsymbol{\theta}_{A\,old}$ are the actor weights before starting a round of policy updates, B is a batch of trajectories collected with $\pi_{\boldsymbol{\theta}_{A\,old}}$, $\hat{A}_t$ is an estimator for the advantage function at timestep t, $\mathbf{H}(\cdot)$ denotes the entropy and ϵ and β_H are hyperparameters controlling clipping and the entropy bonus. The critic minimises

$$\ell_V(\boldsymbol{\theta}_C) = \frac{1}{|B|} \sum_{o_t \in B} (\hat{V}_{\boldsymbol{\theta}_C}(o_t) - \hat{V}_t)^2, \quad (2)$$

where $\hat{V}_t$ are value targets. Both $\hat{A}$ and $\hat{V}$ are computed using GAE (Schulman et al., 2016). PPG performs an auxiliary phase after conducting PPO updates over N_π policy phases. To prevent overfitting, the auxiliary phase fine-tunes the critic and distills value information into the representation from much larger trajectory batches $B_{aux} = \bigcup_{i \in 1, \ldots, N_\pi} B_i$, using the loss $\ell_{\text{joint}} = \ell_V + \ell_{aux}$, with

$$\ell_{aux}(\boldsymbol{\theta}_A) = \frac{1}{|B_{aux}|} \sum_{(a_t, o_t) \in B_{aux}} (\hat{V}_{\boldsymbol{\theta}_A}^{aux}(o_t) - \hat{V}_t)^2 + \beta_c D_{\text{KL}}(\pi_{\boldsymbol{\theta}_{A\,old}}(a_t|o_t) \| \pi_{\boldsymbol{\theta}_A}(a_t|o_t)), \quad (3)$$

where β_c controls the distortion of the policy. When decoupled, $\hat{V}^{aux} \triangleq v^{aux} \circ \phi_A$ distills value information into representation parameters $\boldsymbol{\eta}_A$ through an additional head v^{aux}. When coupled, $v^{aux} \equiv \hat{v}$, and a stop-gradient operation on ℓ_V ensures $\boldsymbol{\eta}$ is updated by the critic during the auxiliary phase only.

Mutual information. We study the information embedded in features z outputted by ϕ. To do so, we propose metrics based on the mutual information $\mathrm{I}(X; Y)$, measuring the information shared between sets of random variables X and Y, defined as

$$\mathrm{I}(X; Y) = \mathbf{H}(X) + \mathbf{H}(Y) - \mathbf{H}(X, Y) = \sum_{\mathbb{X}} \sum_{\mathbb{Y}} p(x, y) \log \frac{p(x, y)}{p(x)p(y)}, \quad (4)$$

where integrals replace sums for continuous quantities. $\mathrm{I}(X; Y)$ is symmetric, and quantifies how much information about Y is obtained by observing X, and vice versa. Similarly, the conditional mutual information $\mathrm{I}(X; Y | Z)$ measures the information shared between X and Y that does not depend on Z. We measure mutual information using the k-nearest neighbors entropy estimator proposed by Kraskov et al. (2004) and extended to pairings of continuous and discrete variables by Ross (2014). We briefly introduce notation for random variables used in following sections. $L \sim P(\mathrm{c})$ denotes the set of training levels drawn from the CMDP context distribution. A, R, O,

O', X and X' are sets constructed from n transitions $(a_t, r_t, o_t, o_{t+1}, x_t, x_{t+1})$ uniformly sampled from a batch of trajectories collected in L using policy π. Z and Z' are latents features, with $z = \phi(o), z' = \phi(o')$. We construct V using the rewards obtained from t until episode termination, with $v_t = \sum_{\bar{t}=t}^{T} \gamma^{\bar{t}-t} r_{\bar{t}}$.

3 CATEGORISING AND QUANTIFYING THE INFORMATION EXTRACTED BY LEARNED REPRESENTATIONS

To conduct our analysis of the respective functions of the actor and critic representations, we analyse the information being extracted from observations at agent convergence. We propose four mutual information metrics to measure information extracted about the identity of the current training level, the value function, and the inverse and forward dynamics of the environment. Each metric relates to quantities relevant to the actor and critic's respective learning objectives, and to the agent's generalisation performance. They are introduced in turn below.

Overfitting. Our first metric, $I(Z; L)$, quantifies overfitting of the actor and critic representations to the set of training levels, as it measures how easy it is to infer the identity of the current level from Z. We follow a similar reasoning as Garcin et al. (2024) to derive an upper bound for the generalisation error that is proportional to $I(Z_A; L)$.[1]

Theorem 3.1. *The difference in returns achieved in train levels and under the full distribution, or generalisation error, has an upper bound that depends on $I(Z_A; L)$, with*

$$\mathbb{E}_{c \sim \mathcal{U}(L), x_0 \sim \mathcal{P}_0(c)}[V^\pi(x_0)] - \mathbb{E}_{c \sim P(c), x_0 \sim \mathcal{P}_0(c)}[V^\pi(x_0)] \leq \sqrt{\frac{2D^2}{|L|} \times I(Z_A; L)}, \quad (5)$$

where $c \sim \mathcal{U}(L)$ indicates c is sampled uniformly over levels in L, D is a constant such that $|V^\pi(x)| \leq D/2, \forall x, \pi$ and Z_A is the output space of the actor's learned representation.

Value information. The second metric quantifies $I(Z; V)$, the mutual information between Z and state values. While a high $I(Z_C; V)$ facilitates the minimisation of ℓ_V (Equation (2)), we wish to understand whether increasing $I(Z_A; V)$ is always desirable. In fact, we find an apparent contradiction on this matter in prior work: Cobbe et al. (2021) and Wang et al. (2023) report that value distillation into the actor's representation (which implies a high $I(Z_A; V)$) improves sample efficiency and generalisation of coupled and decoupled PPG agents, whereas Raileanu & Fergus (2021) and Garcin et al. (2024) report a positive correlation between generalisation and a high ℓ_V for coupled PPO agents (which implies a low $I(Z_A; V)$).

Dynamics in the latent space. The remaining two metrics investigate the transition dynamics $\mathcal{T}_z : \mathbb{Z} \times \mathbb{A} \to \mathscr{P}(\mathbb{Z})$ within the latent state space $\mathbb{Z}$ spanned by the representation. We will see in later sections that the *reduced MDP* $(\mathbb{Z}, \mathbb{A}, \mathcal{T}_z, R_z, \gamma)$ spanned by the actor or critic's representation tend to have distinct $\mathcal{T}_z$, which often markedly differ from the transition dynamics $\mathcal{T}$ in the original environment. $I(Z; Z')$ measures how easy it is to differentiate a latent pair $(\phi(o), \phi(o'))$ obtained from consecutive observations from a latent pair obtained from non-consecutive observations. $I((Z, Z'); A)$ quantifies how easy it is to predict the action taken during transition $\langle o, a, o' \rangle$ given the pair $(\phi(o), \phi(o'))$. In Theorem 3.2, we establish that $\mathcal{T}_z$ maintains the *Markov property* of the original MDP when both of these metrics attain their theoretical maximum.[2]

Theorem 3.2. *if $\mathcal{T} : \mathbb{X} \times \mathbb{A} \to \mathscr{P}(\mathbb{X})$ satisfies the Markov property, and we have $I((X, X'); A) = I((Z, Z'); A)$ and $I(X; X') = I(Z; Z')$ for any X, X', A, Z, Z' collected using policy π, then $\mathcal{T}_z : \mathbb{Z} \times \mathbb{A} \to \mathscr{P}(\mathbb{Z})$ satisfies the Markov property when following π. $\mathcal{T}_z$ always satisfies the Markov property if the above conditions hold for any π.*

Given that ϕ only induces $\mathcal{T}_z$ for the current π in the on-policy setting, we make the distinction between $\mathcal{T}_z$ being Markov when following π and the more general notion of $\mathcal{T}_z$ being Markov when following any policy. Crucially, Theorem 3.2 generalises the equivalence relations obtained by Allen

---

[1]Proofs for the theoretical results presented in this work are provided in Appendix A.

[2]The Markov property is satisfied for a MDP $(\mathbb{Z}, \mathbb{A}, \mathcal{T}_z, R_z, \gamma)$ if and only if $\mathcal{T}_z^{(k)}(z_{t+1}|\{a_{t-i}, z_{t-i}\}_{i=0}^k) = \mathcal{T}_z(z_{t+1}|a_t, z_t)$ and $R_z^{(k)}(z_{t+1}|\{a_{t-i}, z_{t-i}\}_{i=0}^k) = R_z(z_{t+1}|a_t, z_t), \forall a \in \mathbb{A}, z \in \mathbb{Z}, k \geq 1$.
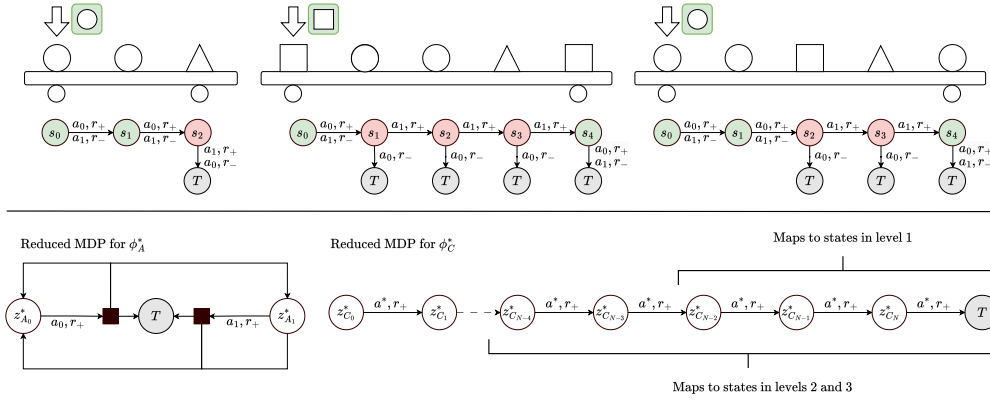
Figure 2: (Top) the initial observations and state spaces of three levels from the assembly line environment in §4. (Bottom) the reduced MDPs spanned by ϕ_A^* and ϕ_C^*.

et al. (2021) to continuous metrics. As such, $\mathrm{I}((Z, Z'); A)$ and $\mathrm{I}(Z; Z')$ quantify how close *any* ϕ comes to have $\mathcal{T}_z$ satisfy the Markov property. They remain applicable in settings in which it isn't practical (or even possible) for $\mathcal{T}_z$ to satisfy the Markov property, e.g. when ϕ has finite capacity and bottlenecks how much information can be extracted from raw observations, or when observations are not Markov.[3]

4 INFORMATION SPECIALISATION IN ACTOR AND CRITIC REPRESENTATIONS

Raileanu & Fergus (2021); Cobbe et al. (2021) have attributed the performance improvements obtained from decoupled architectures to the disappearance of gradient interference between the actor and critic, and to the critic tolerating a higher degree of sample reuse than the actor before overfitting. We propose a different interpretation: given their different learning objectives, the actor's and critic's *optimal representations* (defined below) prioritise different types of information from the environment. While not incompatible with prior interpretations, our claim is stronger. We posit that an optimal (or near-optimal) representation for both the actor and critic will generally be impossible under a shared architecture.

Definition 4.1. *Given the model $m \triangleq f_{\boldsymbol{\omega}} \circ \phi$ and associated loss $\ell_m(\boldsymbol{\omega}, \phi)$, an optimal representation $\phi^* : \mathbb{O} \to \mathbb{Z}^*$ satisfies the conditions:*

1. **Optimality conservation.** $\min_{\boldsymbol{\omega}} \ell_m(\boldsymbol{\omega}, \phi^*) = \min_{\boldsymbol{\omega}, \phi} \ell_m(\boldsymbol{\omega}, \phi)$

2. **Maximal compression.** $\phi^* \in \arg\min_{\tilde{\Phi}} |\mathbb{Z}^*|$, *with $\tilde{\Phi}$ the set of all ϕ satisfying condition 1.*

We will provide theoretical insights on the respective specialisations and mutual incompatibility of ϕ_A^* and ϕ_C^*, which we further highlight through a motivating example. In our example, depicted in Figure 2, the agent inspects parts for defects on an assembly line. The agent is trained on a set L of levels drawn from $P(\mathrm{c})$. A level is characterised by a particular combination of part specifications, number and ordering, each part having a probability P^F of being defective. At each timestep, the agent observes the part specifications for the current level, which parts are on the assembly line and which part is up for inspection. The agent picks action $a \in \mathbb{A} = \{a_0 = accept, a_1 = reject\}$ and moves to the next part. It receives a reward $R = r_+$ when correctly accepting/rejecting a good/defective part and $R = r_-$ when it makes a mistake, with $r_+ > r_-$. The episode terminates early when the agent accepts a defective part, otherwise it terminates after N_c timesteps, where N_c is the number of parts in level $c \in L$.

---

[3]In contrast, Allen et al. (2021) assume observations are always Markov.

4.1 THE ACTOR'S OPTIMAL REPRESENTATION

The combinatorial explosion of possible specifications and part assortments means ϕ_A^* should ideally map observations to a *reduced MDP* spanning a much smaller state space that in the original environment. However, ϕ_A^* should still provide the information necessary to select the optimal action at each timestep of each level, including those not in the training set.

Dynamics of the reduced MDP. Under our definition, the mapping

$$\phi_A^*(o) = \begin{cases} z_{A0}^*, & \text{if } a^* = a_0 \\ z_{A1}^*, & \text{if } a^* = a_1. \end{cases} \tag{6}$$

satisfies the conditions for being an optimal representation, and spans the reduced MDP in Figure 2 (bottom left). This reduced MDP describes the perceived environment dynamics when only observing the latent states in $\mathbb{Z}_A^*$. By construction, $I((Z_A^*, Z_A^{*\prime}); A)$ is guaranteed to be maximised when following the optimal policy. We note that, even if $I(X; X')$ is maximised under π^* in the original environment, we have $I(Z_A^*; Z_A^{*\prime}) = 0$ in the reduced MDP. In other words, the current reduced state yields no information about the next reduced state, and vice versa.

Overfitting to training levels. In our assembly line example, an *overfit* ϕ_A with high $I(Z_A; L)$ may leverage this information to first identify, and then solve certain levels. This overfit ϕ_A may be optimal over L, but would be heavily biased to the training set, and fail to generalise to unseen levels that do not satisfy certain spurious correlations. For example: "*if there are three objects on the line then I must be in level 1, and, in level 1, I should reject the triangle*". In contrast, a representation that is *invariant* to individual levels, i.e. with $I(Z_A; L) = 0$, guarantees zero generalisation error under Theorem 3.1. Nevertheless, achieving $I(Z_A; L) = 0$ is not achievable under certain conditions, stated in Lemma 4.1.

Lemma 4.1. *$I(Z; L) > 0$ if $I(O; L) > 0$ and $\exists z_k, c_j \in Z \times L$ such that $\mu(z_k | c_j) \neq \mu(z_k)$.*

In our example, $I(O; L) > 0$, since a level can be identified from its observations. We can verify that the second condition holds for ϕ_A^* by inspecting the stationary distributions in a particular level c and over all levels,

$$\mu(z) = \begin{cases} \bar{P}^F, & \text{if } z = z_{A0}^* \\ P^F, & \text{if } z = z_{A1}^* \end{cases} \quad \mu(z|c) = \begin{cases} \bar{P}_c^F, & \text{if } z = z_{A0}^* \\ P_c^F, & \text{if } z = z_{A1}^*, \end{cases} \tag{7}$$

where $\bar{P}^F = 1 - P^F$ and P_c^F is the defect probability when in level c. We may have $P^F \neq P_c^F$, since individual levels do not all have the same distribution of defective parts. In other words, while it is useful to reduce $I(Z_A; L)$ to guard against overfitting, the optimal representation ϕ_A^* may carry some irreducible information about level identities.

Value and dynamics distillation can induce overfitting. we can employ the chain rule of mutual information to decompose the information ϕ captures about some arbitrary quantity Y as

$$I(Z; Y) = I(Z; Y|L) + I(Z; L) - I(Z; L|Y), \tag{8}$$

where $I(Z; Y|L)$ is the *level-invariant* information encoded about Y, and $I(Z; L) - I(Z; L|Y)$ is the *level-specific* information being encoded about Y. Thus, encouraging ϕ_A to capture extraneous information about state values or transition dynamics can cause $I(Z_A; L)$ to increase and promote overfitting. In Lemma 4.2, we show that increasing $I(Z_A; V)$ or $I(Z_A; Z_A')$ (which is not necessary for obtaining an optimal ϕ_A^*, as discussed above) can cause $I(Z_A; L)$ to increase as well.

Lemma 4.2. *$I(Z; L)$ monotonically increases with a) $I(Z; V) - I(Z; V|L)$ and b) $I(Z; Z') - I(Z; Z'|L)$.*

In fact, $I(Z; L)$ will increase when $I(Z; V) > I(Z; V|L)$ (or when $I(Z; Z') > I(Z; Z'|L)$), that is when the information encoded carries a level-specific component. In our example, the higher state values only occur in a subset of levels, since the optimal value for any given state depends on how many parts are left to inspect. State values therefore inherently contain level-specific information, and may induce overfitting if this information is captured by ϕ_A. This challenges the notion that value distillation would systematically improve the actor's representation.

The key implications of the above are 1) While achieving zero $I(Z_A; L)$ is not always possible, a high $I(Z_A; L)$ implies ϕ_A is overfit; 2) Increasing $I(Z_A; Z_A')$ or $I(Z_A; V)$ is not necessary for obtaining ϕ_A^*, and will increase $I(Z_A; L)$ if the information captured is level-specific.
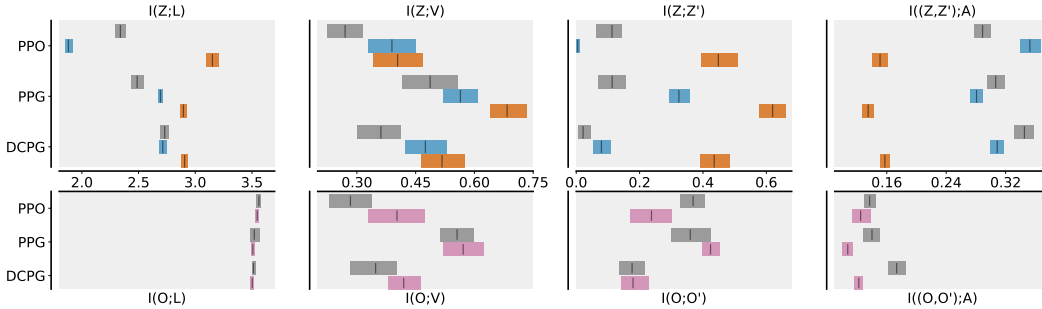
Figure 3: Mean and 95% confidence interval aggregates of $I(Z; \cdot)/I(O; \cdot)$ (top/bottom rows) in Procgen. Gray bars indicate $I(Z; \cdot)/I(O; \cdot)$ for a shared ϕ. Blue and orange bars indicate $I(Z; \cdot)$ measured for ϕ_A and ϕ_C when employing a decoupled architecture. Pink bars indicate $I(O; \cdot)$ measured when using a decoupled architecture. X-axes are shared across top and bottom. For all algorithms, decoupling induces specialisation consistent with §4.

4.2 THE CRITIC'S OPTIMAL REPRESENTATION

ϕ_C^* **has higher I**$(Z; L)$ **than** ϕ_A^***.** The reduced MDP spanned by ϕ_C^* is depicted in Figure 2 (bottom right). In order to ensure perfect value prediction, ϕ_C^* maps each possible optimal state value to a different element in $\mathbb{Z}_C^*$, and it maximises $I(Z_C^*; V)$ by construction. $I(Z_C^*; Z_C^{*\prime})$ is also high due to the recurrence $V^\pi(x) = \mathbb{E}_{a \sim \pi}[R(x, a) + \gamma \mathbb{E}_{x' \sim P^\pi(x'|x)}[V^\pi(x')]]$. This points to V^π being a quantity inherently more level specific than the optimal action for the current state, because V^π encodes information pertaining to all possible future states of the current level. We should then expect that, in general, $I(Z_C^*; L) > I(Z_A^*; L)$, implying that decoupling the actor and critic helps with $I(Z_A; L)$ regularisation.

ϕ_C^* **is not compatible with** π^***.** Paradoxically, while ϕ_C^* would necessitate trajectories collected using the optimal policy in order to be learnt, in our example it is not possible to have an optimal policy that only depends on z_C^*. The information contained in z_C^* is not sufficient for picking the optimal action in any given timestep, and therefore the best response is to always pick a_1 in order to prevent early termination. Therefore, in addition to the information prioritised by ϕ_C^* being in general irrelevant to π^*, employing a shared ϕ with a finite capacity may prevent extracting the necessary information to execute the optimal policy.

4.3 CONFIRMING SPECIALISATION EMPIRICALLY

We conclude this section by studying the representations learned by PPO (Schulman et al., 2017), PPG (Cobbe et al., 2021) and DCPG (Moon et al., 2022), a close variant of PPG that employs delayed value targets to train the critic and for value distillation. We evaluate all algorithms with and without decoupling their representation. We conduct our experiments in Procgen (Cobbe et al., 2020), a benchmark of 16 games designed to measure generalisation in RL. We report our main observations in below, with extended results and details on our methodology included in Appendix C.2.

Figure 4: Effect of parameter scaling in coupled (blue) and decoupled (orange) PPO. Scores normalized by model performance at 0.6M parameters.

Specialisation is consistent with ϕ_A^* **and** ϕ_C^***.** As no algorithm achieves optimal scores in all games, we now consider the suboptimal representations ϕ_A and ϕ_C realistically obtainable by the end of training. In Figure 3, we observe clear specialization upon decoupling consistent with the properties we expect for ϕ_A^* and ϕ_C^*. ϕ_C has high $I(Z; V)$, $I(Z; Z')$ and $I(Z; L)$, while ϕ_A specializes in $I((Z, Z'); A)$.

Decoupling is more parameter efficient. Since decoupled representations fit twice as many parameters, it is fair to wonder whether the performance improvements are mainly caused by the increased model capacity. To test this, we measure performance as we scale model size in a shared and a de-
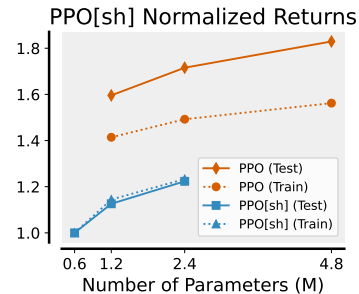
coupled architecture in Figure 4. Surprisingly, the decoupled model turns out to be *more* parameter efficient, and still outperforms a shared model with four times its parameter count.

On Markov representations. According to Theorem 3.2, a representation is considered Markov when both $I((Z, Z'); A)$ and $I(Z; Z')$ are maximized. However, our observations reveal an interesting pattern during decoupling: the actor representation shows an increase in $I((Z_A, Z'_A); A)$ but a decrease in $I(Z_A; Z'_A)$, while the critic representation shows the opposite effect - a decrease in $I((Z_C, Z'_C); A)$ and an increase in $I(Z_C; Z'_C)$. This divergent behavior suggests that neither the actor nor the critic networks inherently benefit from maintaining a Markov representation. This finding aligns with theoretical expectations, as neither ϕ_A nor ϕ_C need be Markov to be optimal. Furthermore, we found no significant correlation between the sum of these mutual information terms $(I((Z, Z'); A) + I(Z; Z'))$ and agent performance, as shown by comparing Figure 7 and Figure 13.

5   REPRESENTATION LEARNING FOR THE ACTOR

In this section, we study how different representation learning objectives affect ϕ_A in PPO, PPG and DCPG. We consider advantage (Raileanu & Fergus, 2021) and dynamics (Moon et al., 2022) prediction, data augmentation (Raileanu et al., 2021) and MICo (Castro et al., 2021), an objective explicitly shaping the latent space to embed differences in state values. We study these objectives in Procgen (Figure 5), and in four continuous control environments with video distractors (McInroe & Garcin, 2025)(Figure 11).

Representation learning impacts information specialisation. As expected, applying auxiliary tasks alters what information is extracted by the representation. Dynamics prediction generally enhances the specialization of ϕ_A by increasing $I((Z, Z'); A)$ while reducing the three other quantities. Conversely, MICo produces the opposite effect - in most cases, it increases $I(Z; Z')$, $I(Z; V)$, and $I(Z; L)$ at the expense of $I((Z, Z'); A)$. The effects of the last two objectives are not as clearcut. Data augmentation produces little change in each quantity, while advantage prediction tends to reduce the measured mutual information, but is inconsistent in the quantities it affects. Performance-wise, data augmentation improves train and test scores for all algorithms; dynamics prediction tends to improve performance for PPG and DCPG; MICo generally decreases performance, and advantage prediction makes no noticeable impact. Based on these findings, we find advisable to not use objectives increasing $I(Z_A; L)$ or playing directly against the specialisation of ϕ_A.

On the importance of the batch size and data diversity. We now turn our attention to an apparent contradiction in the relationship between value distillation and performance. Decoupling PPO, and thus completely forgoing value distillation, leads to improved train and test scores (Figure 13). However, PPG and DCPG perform extensive value distillation (four times as many distillation updates as coupled PPO in our experiments), and achieve significant performance improvements. Crucially, conducting value distillation every N_π policy phases ensures the batch size B_{aux} is N_π times larger than the PPO batch size, greatly increasing its data diversity. Wang et al. (2023) report that increasing diversity is a key driver of performance improvement at equal number of gradient updates. We reproduce their experiment in Figure 12, while also tracking the evolution of $I(Z_A; L)$ and $I(Z_A; V)$ as B_{aux} increases. We find that the increase in $I(Z_A; L)$ in PPG is mainly caused by these additional gradient updates, whereas agent performance and $I(Z_A; V)$ only increase when performing value distillation over large, diverse training batches. Increasing data diversity should promote level-invariant state value information to be distilled into ϕ_A, and we conclude that it is this level invariant information plays a key role in improving agent performance in PPG and DCPG.

Our experiments further reveal that dynamics prediction yields significant performance improvements, but only when applied to algorithms with large batch sizes (specifically in PPG and DCPG, not in PPO). In comparison, data augmentation, which increases data diversity, demonstrates performance benefits across all three algorithms. These findings suggest an important hypothesis: the actor benefits more from encouraging ϕ_A to extract level-invariant information about *any* arbitrary quantity Y, rather than from specifically choosing what that quantity Y should be (such as state values or dynamics).
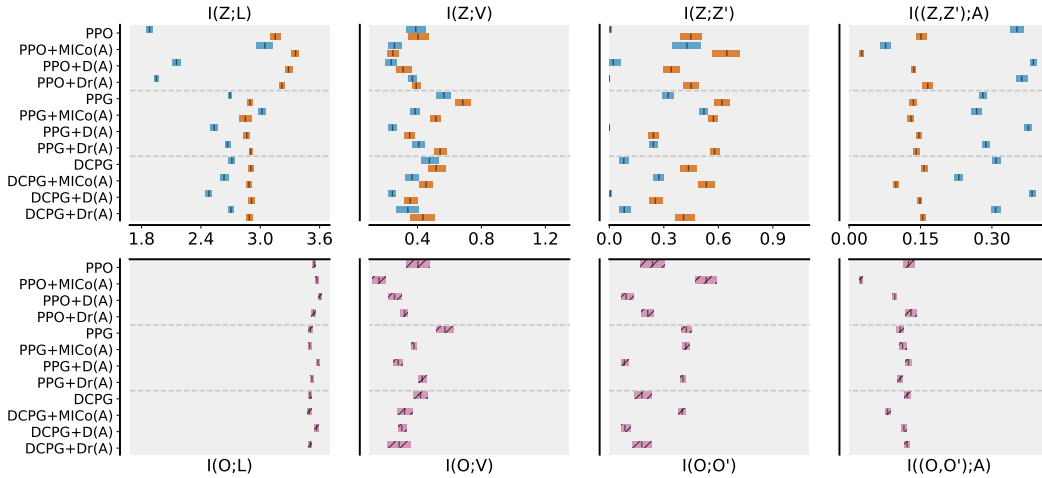
Figure 5: Mean and 95% confidence intervals of $I(Z; \cdot)/I(O; \cdot)$ (top/bottom) for actor (blue) and critic (orange) representations in Procgen. Information measured from agent observations shown in pink. X-axes are shared across top and bottom. Auxiliary tasks shown are MICo, dynamics prediction (D), and data augmentation (Dr) applied to the actor (A).

6 THE CRITIC'S OBJECTIVE INFLUENCES DATA COLLECTION

We now consider how the same set of representation learning objectives affect the critic's representation and present our results in Figures 8 and 11. The effect of a given objective on the information extracted by ϕ_C is consistent with how they would have affected ϕ_A in the previous section. However, we report two surprising findings: a) Without conducting any value distillation, decoupled PPO has a 37% higher $I(Z_A; V)$ than shared PPO (Table 1), and b) the information specialisation of ϕ_C incurred by applying an objective on the critic is often observed in ϕ_A, albeit to a lesser extent. Given that the two representations are decoupled, how can an objective applied to ϕ_C affect ϕ_A?

As we maintain different optimisers for the actor and critic, their only remaining interaction in decoupled PPO is through J_π (Equation (1)): $\hat{A}_t$ being computed from the critic's value estimates. Therefore, at least one of the following hypothesis must hold:

1. **Data collection bias.** Through J^π updates, the critic biases π to collect trajectories containing information relevant to its own learning objective. This information could then leak through ϕ_A because more of this information is contained in its input. In this scenario, it is not necessary for ϕ_A to become more proficient at extracting critic-relevant information.

2. **Implicit knowledge transfer.** The advantage targets in J^π induce information transfer between ϕ_C and ϕ_A when applying the gradients $\nabla_{\boldsymbol{\theta}_A} J^\pi$. Here, ϕ_A becomes proficient at extracting the same information ϕ_C extracts.

The first hypothesis broadly holds in our experiments: in most cases, applying MICo to the critic increases $I(O; V)$ and $I(O; O')$, and applying dynamics prediction increases $I((O, O'); A)$[4]. Furthermore, $I(O; V)$ increases when PPO is decoupled (Figure 3). Without the critic's influence, there would be no direct incentive for the actor to collect data that contains value information, since no value distillation is taking place.

To test the second hypothesis, we measure the *compression efficiency*, applicable whenever $I(O; \cdot) > 0$, and defined as

$$\mathrm{C}(Z; \cdot) = \min\left(\frac{\mathrm{I}(Z; \cdot)}{\mathrm{I}(O; \cdot)}, 1\right). \tag{9}$$

---

[4]In contrast, I(O;L) does not vary significantly, given that the policy does not control which level is played in an episode.

For example, $C(Z_A; V)$ measures the fraction of available information in $I(O; V)$ that is extracted by ϕ_A.[5] In Tables 2 and 3, we report that $C(Z_A; V)$ does not signficantly change between PPO[sh] and decoupled PPO, or when MICo is applied to the critic in decoupled PPO. This result appears to disprove the second hypothesis, at least in PPO. We cannot formally confirm whether implicit knowledge transfer occurs for PPG and DCPG, as explicit knowledge transfer already occurs through value distillation.

Finally, we highlight that this data collection bias generally leads to worse performance (Figure 13). Interestingly, employing different representation learning objectives for the actor and the critic results in surprising interactions. Consider PPO in the Procgen setup: when applied separately, Adv(A) and MICo(C) have respectively a neutral and adverse effect on performance, the latter being caused by the data collection bias caused by the critic. When applied together, they exhibit a sharp performance gain, and bring $I(O; V)$ down (Figure 10). This suggests that certain actor representation objectives could improve performance by cancelling the bias in data collection induced by the critic.

7 RELATED WORK

Representation learning in RL. Representation learning objectives have been used in RL for a variety of reasons such as sample efficiency (Jaderberg et al., 2017; Gelada et al., 2019; Laskin et al., 2020a; Lee et al., 2020; Laskin et al., 2020b), planning (Sekar et al., 2020; McInroe et al., 2024), disentanglement (Dunion et al., 2023b), and generalisation (Higgins et al., 2017; Li et al., 2021). Some works focus on designing metrics motivated by theoretical properties such as bisimulation metrics, pseudometrics, decompositions of MDP components, or successor features (Ferns et al., 2004; Mahadevan & Maggioni, 2007; Dayan, 1993; Castro, 2020; Agarwal et al., 2021; Castro et al., 2021; 2023).

Analysing representations in RL. Despite the large body of research into representation learning objectives in RL, relatively little work has gone into understanding the learned representations themselves (Wang et al., 2024). Several works use linear probing to determine how well learned representations relate to environment or agent properties (Racah & Pal, 2019; Guo et al., 2018; Anand et al., 2019; Zhang et al., 2024). Other works analyse the learned representation functions via saliency maps which help visualise where an agent is "paying attention" (Rosynski et al., 2020; Atrey et al., 2020; Dunion et al., 2023a).

8 CONCLUSION

In this work, we conducted an in-depth analysis of the representations learned by actor and critic networks in on-policy deep reinforcement learning. Our key findings revealed that when decoupled, actor and critic representations specialise in extracting different types of information from the environment. We found that the actor benefits from representation learning objectives that promote extracting level-invariant information. Finally, we discovered that the critic influences policy updates to collect data that is informative for its own learning objective.

We identify three important research directions to be tackled in future work: 1) Broadening this study's scope to cover different network architectures, representation learning objectives, or RL algorithms (such as off-policy RL (Haarnoja et al., 2018)); 2) Employing these findings to design new representation learning objectives for the actor that target level-invariant information; 3) Leveraging the critic's influence on data collection to devise new exploration strategies in online RL.

REPRODUCIBILITY STATEMENT

Reproducibility can be challenging without access to the data generated during experiments. To assist with this, we will make all of our experimental data, including model checkpoints, logged

---

[5]By the data processing inequality we must have $I(O; \cdot) \geq I(Z; \cdot)$, and $C(Z; \cdot)$ cannot be larger than 1. We enforce this upper bound as our estimator sometimes underestimates $I(O; \cdot)$ for high dimensional observations.

data and the code for reproducing the figures in this paper openly available at `https://github.com/francelico/deac-rep`.

REFERENCES

Rishabh Agarwal, Marlos C. Machado, Pablo Samuel Castro, and Marc G. Bellemare. Contrastive behavioral similarity embeddings for generalization in reinforcement learning. In *9th International Conference on Learning Representations, ICLR 2021, Virtual Event, Austria, May 3-7, 2021*. OpenReview.net, 2021. URL `https://openreview.net/forum?id=qda7-sVg84`.

Cameron Allen, Neev Parikh, Omer Gottesman, and George Konidaris. Learning markov state abstractions for deep reinforcement learning. In Marc'Aurelio Ranzato, Alina Beygelzimer, Yann N. Dauphin, Percy Liang, and Jennifer Wortman Vaughan (eds.), *Advances in Neural Information Processing Systems 34: Annual Conference on Neural Information Processing Systems 2021, NeurIPS 2021, December 6-14, 2021, virtual*, pp. 8229–8241, 2021. URL `https://proceedings.neurips.cc/paper/2021/hash/454cecc4829279e64d624cd8a8c9ddf1-Abstract.html`.

Ankesh Anand, Evan Racah, Sherjil Ozair, Yoshua Bengio, Marc-Alexandre Côté, and R. Devon Hjelm. Unsupervised state representation learning in atari. In Hanna M. Wallach, Hugo Larochelle, Alina Beygelzimer, Florence d'Alché-Buc, Emily B. Fox, and Roman Garnett (eds.), *Advances in Neural Information Processing Systems 32: Annual Conference on Neural Information Processing Systems 2019, NeurIPS 2019, December 8-14, 2019, Vancouver, BC, Canada*, pp. 8766–8779, 2019. URL `https://proceedings.neurips.cc/paper/2019/hash/6fb52e71b837628ac16539c1ff911667-Abstract.html`.

Akanksha Atrey, Kaleigh Clary, and David D. Jensen. Exploratory not explanatory: Counterfactual analysis of saliency maps for deep reinforcement learning. In *8th International Conference on Learning Representations, ICLR 2020, Addis Ababa, Ethiopia, April 26-30, 2020*. OpenReview.net, 2020. URL `https://openreview.net/forum?id=rkl3m1BFDB`.

Marc G. Bellemare, Yavar Naddaf, Joel Veness, and Michael Bowling. The arcade learning environment: An evaluation platform for general agents (extended abstract). In Qiang Yang and Michael J. Wooldridge (eds.), *Proceedings of the Twenty-Fourth International Joint Conference on Artificial Intelligence, IJCAI 2015, Buenos Aires, Argentina, July 25-31, 2015*, pp. 4148–4152. AAAI Press, 2015. URL `http://ijcai.org/Abstract/15/585`.

Martín Bertrán, Natalia Martínez, Mariano Phielipp, and Guillermo Sapiro. Instance-based generalization in reinforcement learning. In Hugo Larochelle, Marc'Aurelio Ranzato, Raia Hadsell, Maria-Florina Balcan, and Hsuan-Tien Lin (eds.), *Advances in Neural Information Processing Systems 33: Annual Conference on Neural Information Processing Systems 2020, NeurIPS 2020, December 6-12, 2020, virtual*, 2020. URL `https://proceedings.neurips.cc/paper/2020/hash/82674fc29bc0d9895cee346548c2cb5c-Abstract.html`.

Pablo Samuel Castro. Scalable methods for computing state similarity in deterministic markov decision processes. In *The Thirty-Fourth AAAI Conference on Artificial Intelligence, AAAI 2020, The Thirty-Second Innovative Applications of Artificial Intelligence Conference, IAAI 2020, The Tenth AAAI Symposium on Educational Advances in Artificial Intelligence, EAAI 2020, New York, NY, USA, February 7-12, 2020*, pp. 10069–10076. AAAI Press, 2020. URL `https://aaai.org/ojs/index.php/AAAI/article/view/6564`.

Pablo Samuel Castro, Tyler Kastner, Prakash Panangaden, and Mark Rowland. Mico: Improved representations via sampling-based state similarity for markov decision processes. In Marc'Aurelio Ranzato, Alina Beygelzimer, Yann N. Dauphin, Percy Liang, and Jennifer Wortman Vaughan (eds.), *Advances in Neural Information Processing Systems 34: Annual Conference on Neural Information Processing Systems 2021, NeurIPS 2021, December 6-14, 2021, virtual*, pp. 30113–30126, 2021. URL `https://proceedings.neurips.cc/paper/2021/hash/fd06b8ea02fe5b1c2496fe1700e9d16c-Abstract.html`.

Pablo Samuel Castro, Tyler Kastner, Prakash Panangaden, and Mark Rowland. A kernel perspective on behavioural metrics for markov decision processes. *TMLR*, 2023.

Karl Cobbe, Christopher Hesse, Jacob Hilton, and John Schulman. Leveraging procedural generation to benchmark reinforcement learning. In *Proceedings of the 37th International Conference on Machine Learning, ICML 2020, 13-18 July 2020, Virtual Event*, volume 119 of *Proceedings of Machine Learning Research*, pp. 2048–2056. PMLR, 2020. URL `http://proceedings.mlr.press/v119/cobbe20a.html`.

Karl Cobbe, Jacob Hilton, Oleg Klimov, and John Schulman. Phasic policy gradient. In Marina Meila and Tong Zhang (eds.), *Proceedings of the 38th International Conference on Machine Learning, ICML 2021, 18-24 July 2021, Virtual Event*, volume 139 of *Proceedings of Machine Learning Research*, pp. 2020–2027. PMLR, 2021. URL `http://proceedings.mlr.press/v139/cobbe21a.html`.

Peter Dayan. Improving generalization for temporal difference learning: The successor representation. *Neural Computation*, 5:613–624, 1993.

Mhairi Dunion, Trevor McInroe, Kevin Sebastian Luck, Josiah Hanna, and Stefano V. Albrecht. Conditional mutual information for disentangled representations in reinforcement learning. In Alice Oh, Tristan Naumann, Amir Globerson, Kate Saenko, Moritz Hardt, and Sergey Levine (eds.), *Advances in Neural Information Processing Systems 36: Annual Conference on Neural Information Processing Systems 2023, NeurIPS 2023, New Orleans, LA, USA, December 10 - 16, 2023*, 2023a. URL `http://papers.nips.cc/paper_files/paper/2023/hash/fd750154df5f199f94df897975621306-Abstract-Conference.html`.

Mhairi Dunion, Trevor McInroe, Kevin Sebastian Luck, Josiah P. Hanna, and Stefano V. Albrecht. Temporal disentanglement of representations for improved generalisation in reinforcement learning. In *The Eleventh International Conference on Learning Representations, ICLR 2023, Kigali, Rwanda, May 1-5, 2023*. OpenReview.net, 2023b. URL `https://openreview.net/pdf?id=sPgP6aISLTD`.

Norman Ferns, Prakash Panangaden, and Doina Precup. Metrics for finite markov decision processes. In *Conference on Uncertainty in Artificial Intelligence*, 2004.

Samuel Garcin, James Doran, Shangmin Guo, Christopher G. Lucas, and Stefano V. Albrecht. DRED: zero-shot transfer in reinforcement learning via data-regularised environment design. In *Forty-first International Conference on Machine Learning, ICML 2024, Vienna, Austria, July 21-27, 2024*. OpenReview.net, 2024. URL `https://openreview.net/forum?id=uku9r6RROl`.

Carles Gelada, Saurabh Kumar, Jacob Buckman, Ofir Nachum, and Marc G. Bellemare. Deepmdp: Learning continuous latent space models for representation learning. In Kamalika Chaudhuri and Ruslan Salakhutdinov (eds.), *Proceedings of the 36th International Conference on Machine Learning, ICML 2019, 9-15 June 2019, Long Beach, California, USA*, volume 97 of *Proceedings of Machine Learning Research*, pp. 2170–2179. PMLR, 2019. URL `http://proceedings.mlr.press/v97/gelada19a.html`.

Zhaohan Daniel Guo, Mohammad Gheshlaghi Azar, Bilal Piot, Bernardo A. Pires, and Rémi Munos. Neural predictive belief representations. *ArXiv preprint*, abs/1811.06407, 2018. URL `https://arxiv.org/abs/1811.06407`.

Tuomas Haarnoja, Aurick Zhou, Pieter Abbeel, and Sergey Levine. Soft actor-critic: Off-policy maximum entropy deep reinforcement learning with a stochastic actor. In Jennifer G. Dy and Andreas Krause (eds.), *Proceedings of the 35th International Conference on Machine Learning, ICML 2018, Stockholmsmässan, Stockholm, Sweden, July 10-15, 2018*, volume 80 of *Proceedings of Machine Learning Research*, pp. 1856–1865. PMLR, 2018. URL `http://proceedings.mlr.press/v80/haarnoja18b.html`.

Irina Higgins, Arka Pal, Andrei A. Rusu, Loïc Matthey, Christopher Burgess, Alexander Pritzel, Matthew Botvinick, Charles Blundell, and Alexander Lerchner. DARLA: improving zero-shot transfer in reinforcement learning. In Doina Precup and Yee Whye Teh (eds.), *Proceedings of the 34th International Conference on Machine Learning, ICML 2017, Sydney, NSW, Australia, 6-11 August 2017*, volume 70 of *Proceedings of Machine Learning Research*, pp. 1480–1490. PMLR, 2017. URL `http://proceedings.mlr.press/v70/higgins17a.html`.

Shengyi Huang, Rousslan Fernand Julien Dossa, Chang Ye, Jeff Braga, Dipam Chakraborty, Kinal Mehta, and João G.M. Araújo. Cleanrl: High-quality single-file implementations of deep reinforcement learning algorithms. *Journal of Machine Learning Research*, 23(274):1–18, 2022. URL http://jmlr.org/papers/v23/21-1342.html.

Max Jaderberg, Volodymyr Mnih, Wojciech Marian Czarnecki, Tom Schaul, Joel Z. Leibo, David Silver, and Koray Kavukcuoglu. Reinforcement learning with unsupervised auxiliary tasks. In *5th International Conference on Learning Representations, ICLR 2017, Toulon, France, April 24-26, 2017, Conference Track Proceedings*. OpenReview.net, 2017. URL https://openreview.net/forum?id=SJ6yPD5xg.

Minqi Jiang, Edward Grefenstette, and Tim Rocktäschel. Prioritized level replay. In Marina Meila and Tong Zhang (eds.), *Proceedings of the 38th International Conference on Machine Learning, ICML 2021, 18-24 July 2021, Virtual Event*, volume 139 of *Proceedings of Machine Learning Research*, pp. 4940–4950. PMLR, 2021. URL http://proceedings.mlr.press/v139/jiang21b.html.

Robert Kirk, Amy Zhang, Edward Grefenstette, and Tim Rocktäschel. A survey of zero-shot generalisation in deep reinforcement learning. *Journal of Artificial Intelligence Research*, 76:201–264, 2023.

Alexander Kraskov, Harald Stögbauer, and Peter Grassberger. Estimating mutual information. *Physical Review E—Statistical, Nonlinear, and Soft Matter Physics*, 69(6):066138, 2004.

Michael Laskin, Kimin Lee, Adam Stooke, Lerrel Pinto, Pieter Abbeel, and Aravind Srinivas. Reinforcement learning with augmented data. In Hugo Larochelle, Marc'Aurelio Ranzato, Raia Hadsell, Maria-Florina Balcan, and Hsuan-Tien Lin (eds.), *Advances in Neural Information Processing Systems 33: Annual Conference on Neural Information Processing Systems 2020, NeurIPS 2020, December 6-12, 2020, virtual*, 2020a. URL https://proceedings.neurips.cc/paper/2020/hash/e615c82aba461681ade82da2da38004a-Abstract.html.

Michael Laskin, Aravind Srinivas, and Pieter Abbeel. CURL: contrastive unsupervised representations for reinforcement learning. In *Proceedings of the 37th International Conference on Machine Learning, ICML 2020, 13-18 July 2020, Virtual Event*, volume 119 of *Proceedings of Machine Learning Research*, pp. 5639–5650. PMLR, 2020b. URL http://proceedings.mlr.press/v119/laskin20a.html.

Kuang-Huei Lee, Ian Fischer, Anthony Liu, Yijie Guo, Honglak Lee, John Canny, and Sergio Guadarrama. Predictive information accelerates learning in RL. In Hugo Larochelle, Marc'Aurelio Ranzato, Raia Hadsell, Maria-Florina Balcan, and Hsuan-Tien Lin (eds.), *Advances in Neural Information Processing Systems 33: Annual Conference on Neural Information Processing Systems 2020, NeurIPS 2020, December 6-12, 2020, virtual*, 2020. URL https://proceedings.neurips.cc/paper/2020/hash/89b9e0a6f6d1505fe13dea0f18a2dcfa-Abstract.html.

Bonnie Li, Vincent François-Lavet, Thang Doan, and Joelle Pineau. Domain adversarial reinforcement learning. *ArXiv preprint*, abs/2102.07097, 2021. URL https://arxiv.org/abs/2102.07097.

Sridhar Mahadevan and Mauro Maggioni. Proto-value functions: A laplacian framework for learning representation and control in markov decision processes. *JMLR*, 2007.

Trevor McInroe and Samuel Garcin. Pixelbrax: Learning continuous control from pixels end-to-end on the gpu. *ArXiv preprint*, abs/2502.00021, 2025. URL https://arxiv.org/abs/2502.00021.

Trevor McInroe, Lukas Schäfer, and Stefano V. Albrecht. Multi-horizon representations with hierarchical forward models for reinforcement learning. *TMLR*, 2023.

Trevor McInroe, Adam Jelley, Stefano V. Albrecht, and Amos Storkey. Planning to go out-of-distribution in offline-to-online reinforcement learning. In *RLC*, 2024.

Seungyong Moon, JunYeong Lee, and Hyun Oh Song. Rethinking value function learning for generalization in reinforcement learning. In Sanmi Koyejo, S. Mohamed, A. Agarwal, Danielle Belgrave, K. Cho, and A. Oh (eds.), *Advances in Neural Information Processing Systems 35: Annual Conference on Neural Information Processing Systems 2022, NeurIPS 2022, New Orleans, LA, USA, November 28 - December 9, 2022*, 2022. URL http://papers.nips.cc/paper_files/paper/2022/hash/e19ab2dde2e60cf68d1ded18c38938f4-Abstract-Conference.html.

Evan Racah and Christopher Pal. Supervise thyself: Examining self-supervised representations in interactive environments. *ArXiv preprint*, abs/1906.11951, 2019. URL https://arxiv.org/abs/1906.11951.

Roberta Raileanu and Rob Fergus. Decoupling value and policy for generalization in reinforcement learning. In Marina Meila and Tong Zhang (eds.), *Proceedings of the 38th International Conference on Machine Learning, ICML 2021, 18-24 July 2021, Virtual Event*, volume 139 of *Proceedings of Machine Learning Research*, pp. 8787–8798. PMLR, 2021. URL http://proceedings.mlr.press/v139/raileanu21a.html.

Roberta Raileanu, Max Goldstein, Denis Yarats, Ilya Kostrikov, and Rob Fergus. Automatic data augmentation for generalization in reinforcement learning. In Marc'Aurelio Ranzato, Alina Beygelzimer, Yann N. Dauphin, Percy Liang, and Jennifer Wortman Vaughan (eds.), *Advances in Neural Information Processing Systems 34: Annual Conference on Neural Information Processing Systems 2021, NeurIPS 2021, December 6-14, 2021, virtual*, pp. 5402–5415, 2021. URL https://proceedings.neurips.cc/paper/2021/hash/2b38c2df6a49b97f706ec9148ce48d86-Abstract.html.

Brian C Ross. Mutual information between discrete and continuous data sets. *PloS one*, 9(2): e87357, 2014.

Matthias Rosynski, Frank Kirchner, and Matias Valdenegro-Toro. Are gradient-based saliency maps useful in deep reinforcement learning? *ArXiv preprint*, abs/2012.01281, 2020. URL https://arxiv.org/abs/2012.01281.

John Schulman, Philipp Moritz, Sergey Levine, Michael I. Jordan, and Pieter Abbeel. High-dimensional continuous control using generalized advantage estimation. In Yoshua Bengio and Yann LeCun (eds.), *4th International Conference on Learning Representations, ICLR 2016, San Juan, Puerto Rico, May 2-4, 2016, Conference Track Proceedings*, 2016. URL http://arxiv.org/abs/1506.02438.

John Schulman, Filip Wolski, Prafulla Dhariwal, Alec Radford, and Oleg Klimov. Proximal policy optimization algorithms. *arXiv*, 2017.

Max Schwarzer, Ankesh Anand, Rishab Goel, R. Devon Hjelm, Aaron C. Courville, and Philip Bachman. Data-efficient reinforcement learning with self-predictive representations. In *9th International Conference on Learning Representations, ICLR 2021, Virtual Event, Austria, May 3-7, 2021*. OpenReview.net, 2021. URL https://openreview.net/forum?id=uCQfPZwRaUu.

Ramanan Sekar, Oleh Rybkin, Kostas Daniilidis, Pieter Abbeel, Danijar Hafner, and Deepak Pathak. Planning to explore via self-supervised world models. In *Proceedings of the 37th International Conference on Machine Learning, ICML 2020, 13-18 July 2020, Virtual Event*, volume 119 of *Proceedings of Machine Learning Research*, pp. 8583–8592. PMLR, 2020. URL http://proceedings.mlr.press/v119/sekar20a.html.

Austin Stone, Oscar Ramirez, Kurt Konolige, and Rico Jonschkowski. The distracting control suite – a challenging benchmark for reinforcement learning from pixels. *ArXiv preprint*, abs/2101.02722, 2021. URL https://arxiv.org/abs/2101.02722.

Han Wang, Erfan Miahi, Martha White, Marlos C Machado, Zaheer Abbas, Raksha Kumaraswamy, Vincent Liu, and Adam White. Investigating the properties of neural network representations in reinforcement learning. *Artificial Intelligence*, 330:104100, 2024.

Kaixin Wang, Daquan Zhou, Jiashi Feng, and Shie Mannor. PPG reloaded: An empirical study on what matters in phasic policy gradient. In Andreas Krause, Emma Brunskill, Kyunghyun Cho, Barbara Engelhardt, Sivan Sabato, and Jonathan Scarlett (eds.), *International Conference on Machine Learning, ICML 2023, 23-29 July 2023, Honolulu, Hawaii, USA*, volume 202 of *Proceedings of Machine Learning Research*, pp. 36694–36713. PMLR, 2023. URL `https://proceedings.mlr.press/v202/wang23aw.html`.

Jiayi Weng, Min Lin, Shengyi Huang, Bo Liu, Denys Makoviichuk, Viktor Makoviychuk, Zichen Liu, Yufan Song, Ting Luo, Yukun Jiang, Zhongwen Xu, and Shuicheng Yan. Envpool: A highly parallel reinforcement learning environment execution engine. In Sanmi Koyejo, S. Mohamed, A. Agarwal, Danielle Belgrave, K. Cho, and A. Oh (eds.), *Advances in Neural Information Processing Systems 35: Annual Conference on Neural Information Processing Systems 2022, NeurIPS 2022, New Orleans, LA, USA, November 28 - December 9, 2022*, 2022. URL `http://papers.nips.cc/paper_files/paper/2022/hash/8caaf08e49ddbad6694fae067442ee21-Abstract-Datasets_and_Benchmarks.html`.

Denis Yarats, Ilya Kostrikov, and Rob Fergus. Image augmentation is all you need: Regularizing deep reinforcement learning from pixels. In *9th International Conference on Learning Representations, ICLR 2021, Virtual Event, Austria, May 3-7, 2021*. OpenReview.net, 2021a. URL `https://openreview.net/forum?id=GY6-6sTvGaf`.

Denis Yarats, Amy Zhang, Ilya Kostrikov, Brandon Amos, Joelle Pineau, and Rob Fergus. Improving sample efficiency in model-free reinforcement learning from images. In *Thirty-Fifth AAAI Conference on Artificial Intelligence, AAAI 2021, Thirty-Third Conference on Innovative Applications of Artificial Intelligence, IAAI 2021, The Eleventh Symposium on Educational Advances in Artificial Intelligence, EAAI 2021, Virtual Event, February 2-9, 2021*, pp. 10674–10681. AAAI Press, 2021b. URL `https://ojs.aaai.org/index.php/AAAI/article/view/17276`.

Amy Zhang, Rowan Thomas McAllister, Roberto Calandra, Yarin Gal, and Sergey Levine. Learning invariant representations for reinforcement learning without reconstruction. In *9th International Conference on Learning Representations, ICLR 2021, Virtual Event, Austria, May 3-7, 2021*. OpenReview.net, 2021. URL `https://openreview.net/forum?id=-2FCwDKRREu`.

Wancong Zhang, Anthony GX-Chen, Vlad Sobal, Yann LeCun, , and Nicolas Carion. Light-weight probing of unsupervised representations for reinforcement learning. In *RLC*, 2024.

A THEORETICAL RESULTS

Theorem 3.1. *The difference in returns achieved in train levels and under the full distribution, or generalisation error, has an upper bound that depends on $I(Z_A; L)$, with*

$$\mathbb{E}_{c\sim\mathcal{U}(L),x_0\sim\mathcal{P}_0(c)}[V^\pi(x_0)] - \mathbb{E}_{c\sim P(c),x_0\sim\mathcal{P}_0(c)}[V^\pi(x_0)] \leq \sqrt{\frac{2D^2}{|L|} \times I(Z_A; L)}, \qquad (5)$$

where $c \sim \mathcal{U}(L)$ indicates c is sampled uniformly over levels in L, D is a constant such that $|V^\pi(x)| \leq D/2, \forall x, \pi$ and Z_A is the output space of the actor's learned representation.

Proof. This result directly follows from a result obtained by Bertrán et al. (2020) and reproduced below.

Theorem A.1. *For any CMDP such that $|V^\pi(x)| \leq D/2, \forall x, \pi$, with D being a constant, then for any set of training levels L, and policy π*

$$\mathbb{E}_{c\sim\mathcal{U}(L),x_0\sim\mathcal{P}_0(c)}[V^\pi(x_0)] - \mathbb{E}_{c\sim P(c),x_0\sim\mathcal{P}_0(c)}[V^\pi(x_0)] \leq \sqrt{\frac{2D^2}{|L|} \times I(\pi; L)}, \qquad (10)$$

Then, as $\pi \triangleq f \circ \phi_A$, by the data processing inequality we always have $I(\pi; L) \le I(Z_A; L)$, and therefore,

$$\mathbb{E}_{c \sim \mathcal{U}(L), x_0 \sim \mathcal{P}_0(c)}[V^\pi(x_0)] - \mathbb{E}_{c \sim P(c), x_0 \sim \mathcal{P}_0(c)}[V^\pi(x_0)] \le \sqrt{\frac{2D^2}{|L|} \times I(\pi; L)}$$

$$\le \sqrt{\frac{2D^2}{|L|} \times I(Z_A; L)}$$

.

Garcin et al. (2024) follow the same reasoning and obtain an equivalent result, without restating the bound.

$\square$

Theorem 3.2. *if* $\mathcal{T} : \mathbb{X} \times \mathbb{A} \to \mathscr{P}(\mathbb{X})$ *satisfies the Markov property, and we have* $I((X, X'); A) = I((Z, Z'); A)$ *and* $I(X; X') = I(Z; Z')$ *for any* X, X', A, Z, Z' *collected using policy* π, *then* $\mathcal{T}_z :$ $\mathbb{Z} \times \mathbb{A} \to \mathscr{P}(\mathbb{Z})$ *satisfies the Markov property when following* π. $\mathcal{T}_z$ *always satisfies the Markov property if the above conditions hold for any* π.

Proof. This proof has two part. We first demonstrate that the Inverse Model condition of Theorem A.2 from Allen et al. (2021) (reproduced below) is satisfied if and only if $I((Z, Z'); A) = I((X, X'); A)$. We then show that if $I(Z; Z') = I(X; X')$ then the Density Ratio condition is also satisfied.

Theorem A.2. ϕ *is a Markov representation if the following conditions hold for every timestep* t *and any policy* π:

1. **Inverse Model.** *The inverse dynamic model, defined as* $I(a|s', s) := \frac{\mathcal{T}(s'|a,s)\pi(a|s)}{P^\pi(s'|s)}$, *where* $P^\pi(s'|s) = \sum_{\bar{a} \in \mathbb{A}} \mathcal{T}(s'|\bar{a}, s)\pi(a|s)$, *should be equal in the original and reduced MDPs. That is we have* $P^\pi(a|z', z) = P^\pi(a|s, s'), \forall a \in \mathbb{A}, s, s' \in \mathbb{S}$.

2. **Density Ratio.** *The original and abstract next-state density ratios are equal when conditioned on the same abstract state:* $\frac{P^\pi(z'|z)}{P^\pi(z')} = \frac{P^\pi(s'|z)}{P^\pi(s')}, \forall x' \in \mathbb{S}$, *where* $P^\pi(s'|z) = \sum_{\bar{s} \in \mathbb{S}} P^\pi(s'|\bar{s})\mu(\bar{s}|z)$ *and* $\mu(s|z) = \frac{\mathbf{1}_{\phi(s)=z}P^\pi(s)}{\sum_{\bar{s} \in \mathbb{S}} P^\pi(s|\bar{s})}$. $P^\pi(s'|z)$ *is the probability of transitioning to state* s' *and* $\mu(s|z)$ *is the probability of currently being in state* s *when in latent state* z.

We begin with two observations that are useful for our derivation.

Observation A: Given that any $z \in \mathbb{Z}$ is obtained from the mapping $x \xrightarrow{\Omega} o \xrightarrow{\phi} z$, and that $h \triangleq \phi \circ \Omega$ is a deterministic (but not necessarily invertible) function, each element $x \in \mathbb{X}$ maps to a single element $z \in \mathbb{Z}$. It directly follows that $\forall a, z_1, z_2 \in \mathbb{A} \times \mathbb{Z} \times \mathbb{Z}$, we have

$$p(a, z_1, z_2) = \sum_{x_1, x_2 \in \mathbb{X}^2} p(a, x_1, x_2)\mathbf{1}[z_1, z_2 = h(x_1), h(x_2)]$$

and

$$p(z_1, z_2) = \sum_{x_1, x_2 \in \mathbb{X}^2} p(x_1, x_2)\mathbf{1}[z_1, z_2 = h(x_1), h(x_2)]$$

Observation B: Let $P^\pi(a, x, x')$ be the joint distribution of elements in (A, X, X') collected under policy π, we have $P^\pi(a, x_1, x_2) > 0$ if and only if $a, x_1, x_2 \in (A, X, X')$.

Observation C: Similarly to obs. B, we have $P^\pi(x_1, x_2) > 0$ if and only if $x_1, x_2 \in (X, X')$.

1) *Proving that the Inverse Model condition is satisfied if and only if* $I((Z, Z'); A) = I((X, X'); A)$.

16

The above is equivalent to showing that the Inverse Model condition is satisfied if and only if $\mathbf{H}(A|Z, Z') = \mathbf{H}(A|X, X')$. For $\mathbf{H}(A|Z, Z')$, we have

$$\mathbf{H}(A|Z, Z') = -\sum_{A, Z, Z'} P^\pi(a, z, z') \log P^\pi(a|z, z')$$

$$\text{(from obs. A)} \quad = -\sum_{\mathbb{A} \times \mathbb{Z} \times \mathbb{Z}} \sum_{x_1, x_2 \in \mathbb{X}^2} P^\pi(a, x_1, x_2) \mathbf{1}[z, z' = h(x_1), h(x_2)] \log P^\pi(a|z, z')$$

$$\text{(from obs. B)} \quad = -\sum_{\mathbb{A} \times \mathbb{X} \times \mathbb{X}} P^\pi(a, x, x') \sum_{\mathbb{Z}^2} \mathbf{1}[z, z' = h(x), h(x')] \log P^\pi(a|z, z')$$

$$= -\sum_{\mathbb{A} \times \mathbb{X} \times \mathbb{X}} P^\pi(a, x, x') \log \prod_{\mathbb{Z}^2} P^\pi(a|z, z')^{\mathbf{1}[z, z' = h(x), h(x')]}$$

$$= -\sum_{\mathbb{A} \times \mathbb{X} \times \mathbb{X}} P^\pi(x, x') P^\pi(a|x, x') \log \prod_{\mathbb{Z}^2} P^\pi(a|z, z')^{\mathbf{1}[z, z' = h(x), h(x')]}$$

$$= -\mathbb{E}_{X, X'}\Big[\sum_{\mathbb{A}} P^\pi(a|x, x') \log \prod_{\mathbb{Z}^2} P^\pi(a|z, z')^{\mathbf{1}[z, z' = h(x), h(x')]}\Big]$$

It follows that

$$\mathbf{H}(A|Z, Z') - \mathbf{H}(A|X, X') = \mathbb{E}_{X, X'}\left[\sum_{\mathbb{A}} P^\pi(a|x, x') \log \frac{P^\pi(a|x, x')}{\prod_{\mathbb{Z}^2} P^\pi(a|z, z')^{\mathbf{1}[z, z' = h(x), h(x')]}}\right]$$

$$= \mathbb{E}_{X, X'}[D_{\mathrm{KL}}(P\|Q)],$$

with $P = P^\pi(a|x, x')$ and $Q = \prod_{z, z' \in Z, Z'} P^\pi(a|z, z')^{\mathbf{1}[z, z' = h(x), h(x')]}$. From Gibbs inequality we always have $D_{\mathrm{KL}}(p\|q) \geq 0$, therefore $\mathrm{I}((Z, Z'); A) = \mathrm{I}((X, X'); A)$ if and only if $D_{\mathrm{KL}}(P\|Q) = 0$ $\forall x, x' \in X, X'$, which is the case if and only if $P = Q$ almost μ-everywhere.

From observation A, any $x_1, x_2 \in \mathbb{X}^2$ maps to exactly one pair $z_1, z_2 \in \mathbb{Z}^2$, and by construction of X, X', Z, Z', for any pair $x, x' \in X, X'$, we must have $Q = \prod_{\bar{z}, \bar{z}' \in \mathbb{Z}^2} P^\pi(a|\bar{z}, \bar{z}')^{\mathbf{1}[\bar{z}, \bar{z}' = h(x), h(x')]} = P^\pi(a|z, z')$, with z, z' being the corresponding pair in Z, Z'.

Therefore $\mathrm{I}((Z, Z'); A) = \mathrm{I}((X, X'); A)$ if and only if $P^\pi(a|x, x') = P^\pi(a|z, z') \forall x, x', z, z' \in X, X', Z, Z'$, and we recover the Inverse Model condition.

Conversely, if the Inverse Model condition is not satisfied, then $\exists x, x', z, z', a \in X, X', Z, Z', A$ for which $P \neq Q$. Then $D_{\mathrm{KL}}(P\|Q) > 0$ at x, x' and $\mathrm{I}((Z, Z'); A) < \mathrm{I}((X, X'); A)$.

2) *Proving that the Density Ratio condition is satisfied if* $\mathrm{I}(Z; Z') = \mathrm{I}(X; X')$.

We first show that satisfying

$$\frac{P^\pi(x'|x)}{P^\pi(x')} = \frac{P^\pi(z'|z)}{P^\pi(z')} \quad \forall x, x', z, z' \in X, X', Z, Z' \tag{11}$$

is sufficient for satisfying the Density Ratio condition $\frac{P^\pi(x'|z)}{P^\pi(x')} = \frac{P^\pi(z'|z)}{P^\pi(z')}$. We then show that the condition in Equation (11) holds if and only if $\mathrm{I}(Z; Z') = \mathrm{I}(X; X')$.

i) *Showing the Density Ratio condition holds when Equation* (11) *is satisfied.* First we notice that, $\forall x', z \in X', Z$, we have

$$P^\pi(x'|z) = \sum_{\bar{x} \in \mathbb{X}} \mathbf{1}[z = h(\bar{x})] P^\pi(x'|\bar{x}) = \mathbb{E}_X[P^\pi(x'|x)].$$

Then, supposing Equation (11) holds, we must have

$$P^\pi(x'|z) = \mathbb{E}_X[P^\pi(x'|x)] = P^\pi(x') \frac{P^\pi(z'|z)}{P^\pi(z')} \quad \forall x', z, z' \in X', Z, Z',$$

and the Density Ratio condition holds.

ii) *Proving Equation* (11) *holds if and only if* $\mathrm{I}(Z; Z') = \mathrm{I}(X; X')$.

We have

$$I(Z; Z') = \sum_{\mathbb{Z}^2} P^\pi(z, z') \log \frac{P^\pi(z'|z)}{P^\pi(z')}$$

$$\text{(from obs. A)} \quad = \sum_{\mathbb{Z}^2} \sum_{x_1, x_2 \in \mathbb{X}^2} P^\pi(x_1, x_2) \mathbf{1}[z, z' = h(x_1), h(x_2)] \log \frac{P^\pi(z'|z)}{P^\pi(z')}$$

$$\text{(from obs. C)} \quad = \sum_{\mathbb{X}^2} P^\pi(x, x') \sum_{\mathbb{Z}^2} \mathbf{1}[z, z' = h(x), h(x')] \log \frac{P^\pi(z'|z)}{P^\pi(z')}$$

$$= \mathbb{E}_{X, X'} \left[\log \prod_{\mathbb{Z}^2} \left(\frac{P^\pi(z'|z)}{P^\pi(z')} \right)^{\mathbf{1}[z, z' = h(x), h(x')]} \right].$$

Then,

$$I(X; X') - I(Z; Z') = \mathbb{E}_{X, X'}[D_{\mathrm{KL}}(P' \| Q')],$$

with

$$P' = \frac{P^\pi(x'|x)}{P^\pi(x')} \quad \text{and} \quad Q = \prod_{\mathbb{Z}^2} \left(\frac{P^\pi(z'|z)}{P^\pi(z')} \right)^{\mathbf{1}[z, z' = h(x), h(x')]}$$

The remainder of this part follows the same structure as for the first part of the proof.

$I(X; X') = I(Z; Z')$ if and only if $\forall x, x' \in X, X', P = Q$ almost μ-everywhere. Any $x_1, x_2 \in \mathbb{X}^2$ maps to exactly one pair $z_1, z_2 \in \mathbb{Z}^2$, and by construction of X, X', Z, Z', for any pair $x, x' \in X, X'$, we must have

$$Q = \prod_{\bar{z}, \bar{z}' \in \mathbb{Z}^2} \left(\frac{P^\pi(\bar{z}'|\bar{z})}{P^\pi(\bar{z}')} \right)^{\mathbf{1}[\bar{z}, \bar{z}' = h(x), h(x')]} = \frac{P^\pi(z'|z)}{P^\pi(z')},$$

with z, z' being the corresponding pair in Z, Z'.

Therefore $I(X; X') = I(Z; Z')$ if and only if $\forall x, x', z, z' \in X, X', Z, Z'$ we have $\frac{P^\pi(x'|x)}{P^\pi(x')} = \frac{P^\pi(z'|z)}{P^\pi(z')}$. Finally, from i) being true, the Density ratio condition must hold. $\qquad \square$

Lemma 4.1. $I(Z; L) > 0$ if $I(O; L) > 0$ and $\exists z_k, c_j \in Z \times L$ such that $\mu(z_k|c_j) \neq \mu(z_k)$.

Proof. Given π is fixed while the batch O is collected, for a single batch the causal interaction between L, O and Z is described by the Markov chain $X \to O \to Z$, where $x = (s, c) \in \mathbb{S} \times L$ and isn't directly observed. By the data processing inequality, $I(L; Z) \leq I(L; O)$, and as such $I(L; O) > 0$ is a necessary condition for $I(L; Z)$ to be positive.

Note that

$$I(L; Z) = \mathbf{H}(L) + \mathbf{H}(Z) - \mathbf{H}(L, Z) = 0 \Leftrightarrow \mathbf{H}(L, Z) = \mathbf{H}(L) + \mathbf{H}(Z),$$

that is, if and only if Z and L are independently distributed. Given the causal relationship between L and Z, $\mu(z|c)$ is well defined $\forall z, c \in Z \times L$. If $\exists z_k, c_j \in Z \times L$ such that $\mu(z_k|c_j) \neq \mu(z_k)$ then Z and L cannot be independently distributed, and $I(L; Z) > 0$. $\qquad \square$

Lemma 4.2. $I(Z; L)$ *monotonically increases with a)* $I(Z; V) - I(Z; V|L)$ *and b)* $I(Z; Z') - I(Z; Z'|L)$.

Proof. Proof for condition a) : By the causal structure $V \leftarrow X \to O \to Z$ and the chain rule of mutual information, we have

$$I(Z; L) = I(Z; V) - I(Z; V|L) + I(Z; L|V),$$

$I(Z; L|V)$ is the information encoded in Z about the training levels that does not depend on V. $I(Z; V) - I(Z; V|L)$ represents the information encoded in Z about state values that is level-specific. If this term increases then $I(Z; L)$ will also increase.
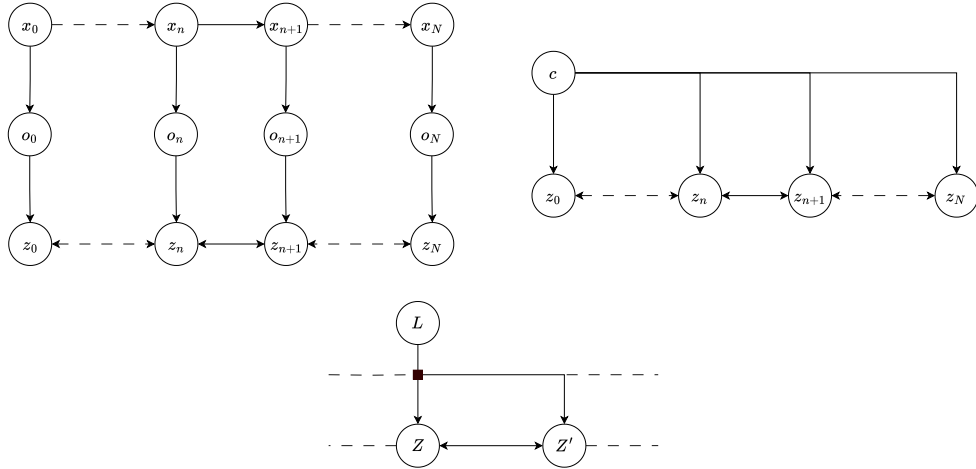
Figure 6: In the top row, left, we depict the causal graph of states, observation and latents obtained over an episode. On the same row we draw a simplified graph that focuses on the relationship between c and $Z_{0:N}$, and utilises the notion that the context remains the same throughout the episode. In the bottom row we draw the resulting causal relationship between L, Z and Z'.

Proof for condition b) : Consider an episode of arbitrary length N collected with policy π. We depict the causal structure that exists between elements in the top row of Figure 6 (elements may be repeated within each sequence). It naturally follows that we have the causal structure depicted in the bottom row when considering all levels in L. By the chain rule of mutual information, we have

$$\mathrm{I}(Z; L) = \mathrm{I}(Z; (Z', L)) - \mathrm{I}(Z; Z'|L) = \mathrm{I}(Z; L|Z') + \mathrm{I}(Z; Z') - \mathrm{I}(Z; Z'|L),$$

and it follows that $\mathrm{I}(Z; L)$ increases with $\mathrm{I}(Z; Z') - \mathrm{I}(Z; Z'|L)$.

$\square$

B ADDITIONAL FIGURES AND TABLES
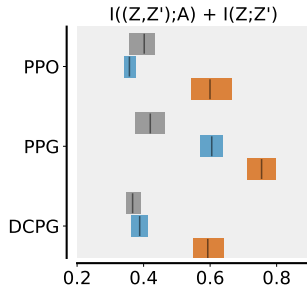

Figure 7: $I((Z, Z'); A) + I(Z; Z')$ for shared (gray), actor (blue) and critic (orange) for PPO, PPG, and DCPG in Procgen.

C IMPLEMENTATION DETAILS

C.1 MUTUAL INFORMATION ESTIMATION

We measure mutual information using the estimator proposed by Kraskov et al. (2004) and later extended to pairings of continuous and discrete variables by Ross (2014). These methods are based
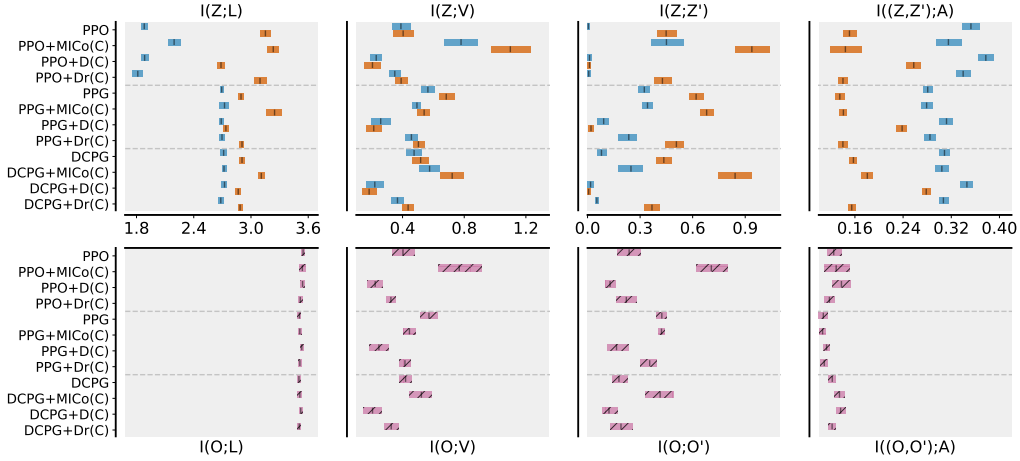
Figure 8: Mutual information measurements for the actor (blue) and critic (orange) for auxiliary losses applied to the critic for PPO, PPG, and DCPG in Procgen. Top/bottom rows are $I(Z; \cdot)/I(O; \cdot)$ with a shared x-axis.

Figure 9: $I(Z; \cdot)$ measurements for the actor (blue) and critic (orange) for auxiliary losses for PPO, PPG, and DCPG in Procgen.

on performing entropy estimation using k-nearest neighbors distances. We use $k = 3$ and determine nearest neighbors by measuring the Euclidian (L_2) distance between points. We checked measurements obtained when using different k and under different metric spaces, and we found that our measurements are broadly invariant to the choice of estimator parameters.

At the end of training we collect a batch of trajectories consisting of 2^{16} timesteps (2^{15} timesteps in Brax) from L. We construct (A, O, O', Z, Z', V, L) from $n = 4096$ timesteps yielding $(a_t, o_t, o_{t+1}, z_t, z_{t+1}, v_t, c_t)$. Subsampling is necessary to compute mutual information estimates in a reasonable time, while ensuring we sample states from most levels in L and at various point of
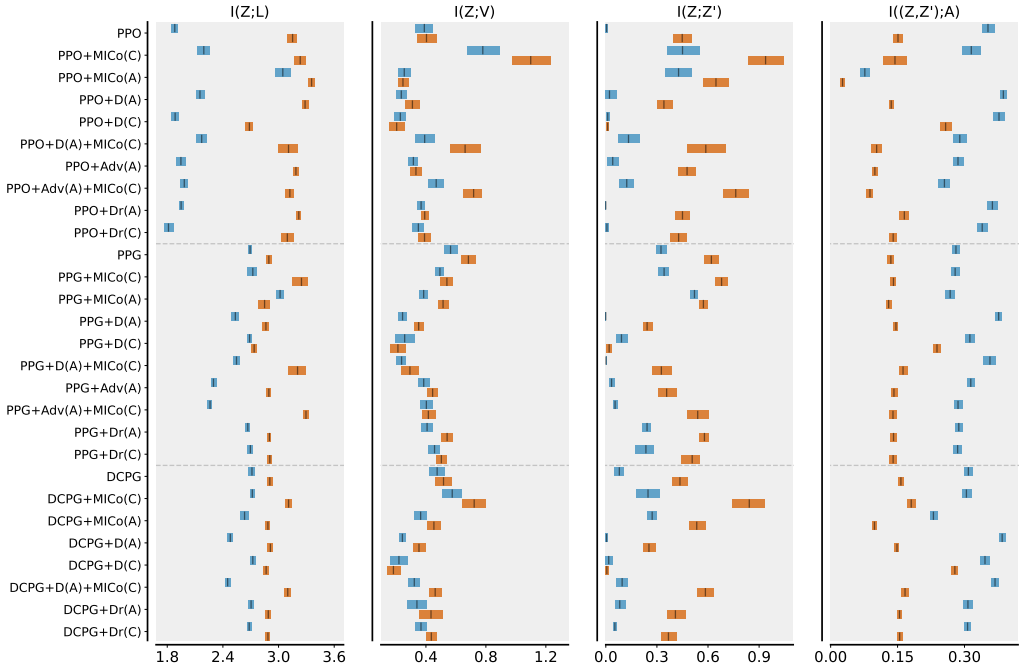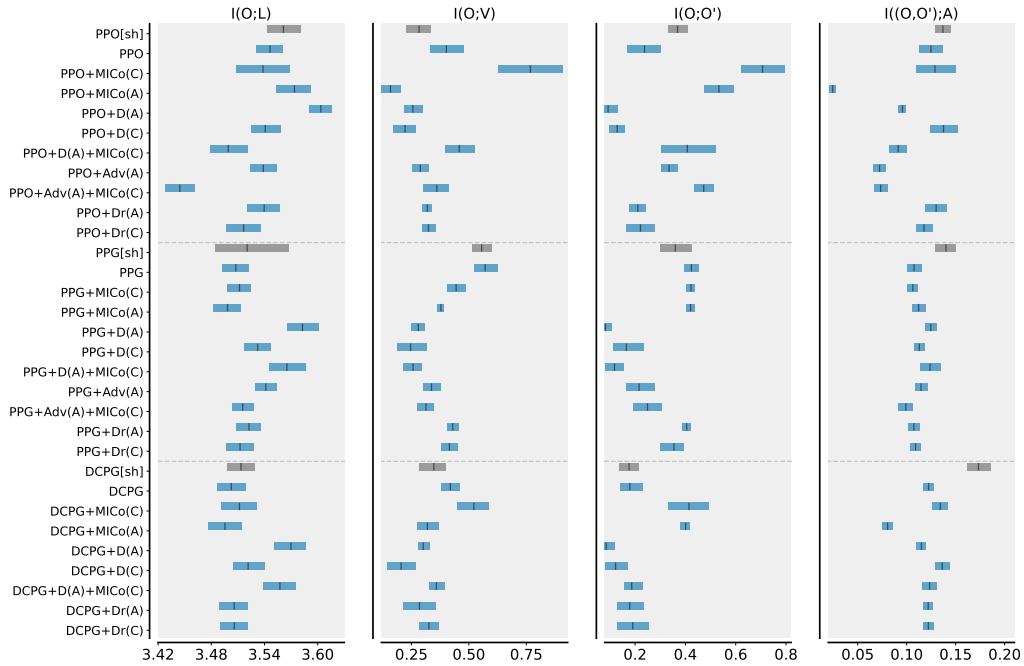
Figure 10: $I(O; \cdot)$ measurements for the actor (blue) and critic (orange) for auxiliary losses for PPO, PPG, and DCPG in Procgen.
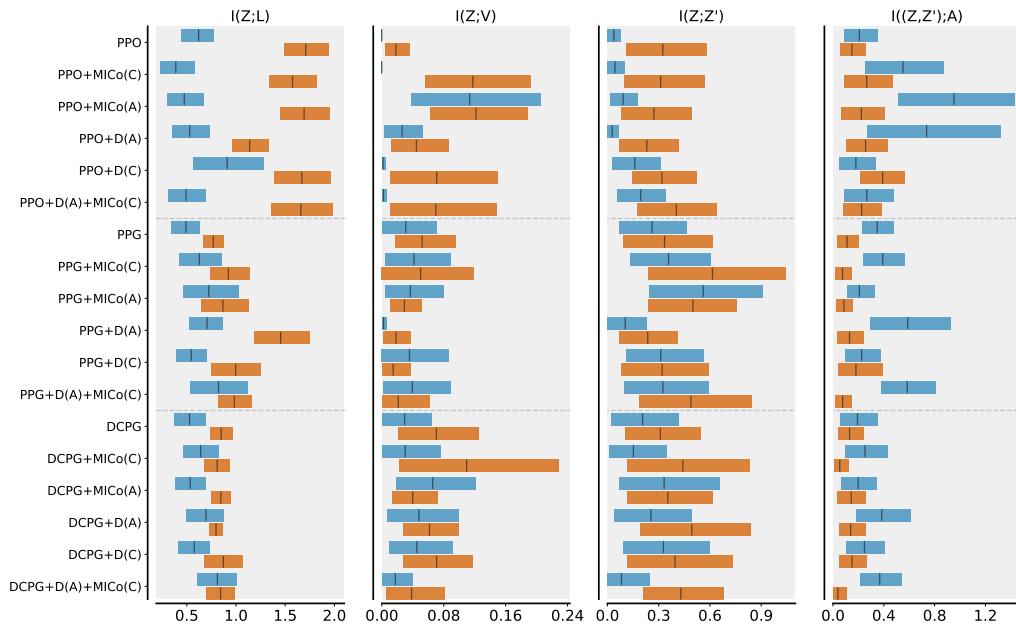
Figure 11: Mutual information measurements for the actor (blue) and critic (orange) for auxiliary losses for PPO, PPG, and DCPG in Brax.

the trajectories followed by the agent in each level. Timesteps are sampled uniformly and without replacement from the batch, after having excluded:

1. Odd timesteps, to ensure O and O' will not overlap (i.e. O contains only even timesteps, and O', being sampled at $t + 1$, contains only odd timesteps).

21
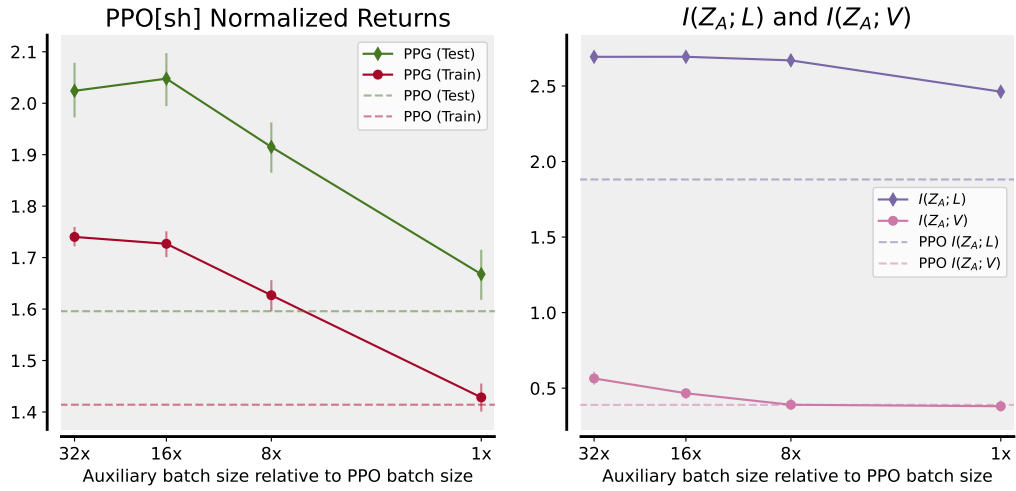
Figure 12: Procgen PPG returns (left) normalized by PPO[sh] performance and mutual information quantities $I(Z_A; L)/I(Z_A; V)$ (right) for varying auxiliary batch size levels.
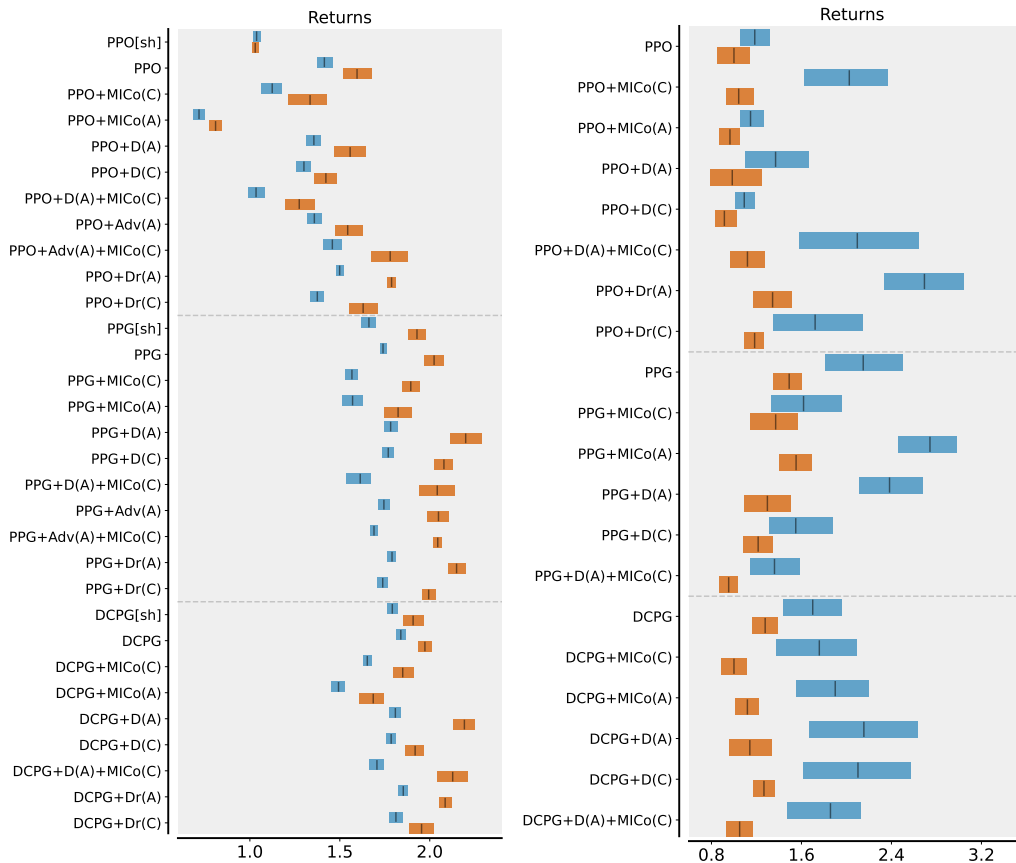
Figure 13: Returns in Procgen (left) and Brax (right).

2. Timesteps corresponding to episode terminations, to ensure the pair $o_t, o_t + 1$ cannot originate from different levels.

3. Timesteps from episodes that have not terminated, to ensure we can always compute v_t.

Table 2: Measurements of compression efficiency $C(Z_A|O;V)$ (Equation (9)) with standard error in Procgen. Statistical significance bolded, determined by Welch's t-test. Results highlighted in red when decoupling decreases $C(Z_A|O;V)$, and highlighted in green when decoupling increases $C(Z_A|O;V)$, otherwise yellow. Coupled architectures are denoted with algorithm name plus "[sh]".

| Algorithm	$C(Z_A|O;V)$	$C(Z_A|O;L)$
PPO[sh]	89.3 ± 2	65.2 ± 3
PPO	90.1 ± 4	$\mathbf{52.3 \pm 3}$
PPG[sh]	85.9 ± 4	70.0 ± 2
PPG	94.1 ± 2	$\mathbf{75.5 \pm 2}$
DCPG[sh]	95.4 ± 2	77.6 ± 2
DCPG	92.3 ± 7	76.4 ± 2

Table 3: Measurements of compression efficiency $C(Z_A|O;\cdot)$ (Equation (9)) of the actor's representation ϕ_A in Procgen. Results highlighted in red when the auxiliary loss decreases the metric relative to the base algorithm, and highlighted in green when the auxiliary loss increases the metric relative to the base algorithm. Auxiliary losses are applied to the actor (A) and critic (C) in the form of dynamics prediction (D), MICo, and advantage distillation (Adv).

Algorithm	$C(Z_A|O;V)$	$C(Z_A|O;L)$	$C((Z_A|O, Z_A'|O');A)$
PPO	90.1 ± 4	52.3 ± 3	99.9 ± 0
PPO+MICo(C)	93.9 ± 2	$\mathbf{60.4 \pm 3}$	99.4 ± 0
PPO+MICo(A)	98.6 ± 1	$\mathbf{84.7 \pm 2}$	$\mathbf{87.5 \pm 5}$
PPO+D(A)	62.6 ± 12	$\mathbf{61.3 \pm 2}$	100.0 ± 0
PPO+D(C)	86.8 ± 7	52.8 ± 3	100.0 ± 0
PPO+D(A)+MICo(C)	76.3 ± 6	$\mathbf{63.7 \pm 3}$	99.5 ± 0
PPO+Adv(A)	96.9 ± 2	53.2 ± 3	100.0 ± 0
PPO+Adv(A)+MICo(C)	$\mathbf{100.0 \pm 0}$	57.0 ± 2	98.5 ± 1
PPO+Dr(A)	89.1 ± 6	54.3 ± 3	100.0 ± 0
PPO+Dr(C)	98.1 ± 1	50.8 ± 3	99.6 ± 0
PPG	94.1 ± 2	75.5 ± 2	100.0 ± 0
PPG+MICo(C)	98.0 ± 1	76.4 ± 2	100.0 ± 0
PPG+MICo(A)	95.4 ± 2	$\mathbf{85.8 \pm 2}$	100.0 ± 0
PPG+D(A)	89.5 ± 4	71.2 ± 2	100.0 ± 0
PPG+D(C)	96.3 ± 2	75.1 ± 2	100.0 ± 0
PPG+D(A)+MICo(C)	85.9 ± 7	71.6 ± 2	100.0 ± 0
PPG+Adv(A)	98.4 ± 1	$\mathbf{63.3 \pm 2}$	100.0 ± 0
PPG+Adv(A)+MICo(C)	99.4 ± 1	$\mathbf{62.9 \pm 2}$	100.0 ± 0
PPG+Dr(A)	91.3 ± 3	74.9 ± 2	100.0 ± 0
PPG+Dr(C)	93.1 ± 6	75.6 ± 2	100.0 ± 0
DCPG	92.3 ± 7	76.4 ± 2	100.0 ± 0
DCPG+MICo(C)	98.1 ± 1	76.6 ± 2	100.0 ± 0
DCPG+MICo(A)	91.7 ± 3	74.3 ± 2	100.0 ± 0
DCPG+D(A)	80.9 ± 4	$\mathbf{69.9 \pm 2}$	100.0 ± 0
DCPG+D(C)	97.8 ± 1	76.3 ± 2	100.0 ± 0
DCPG+D(A)+MICo(C)	83.4 ± 5	$\mathbf{69.6 \pm 2}$	100.0 ± 0
DCPG+Dr(A)	97.5 ± 2	76.7 ± 2	100.0 ± 0

C.2 PROCGEN

The Procgen Benchmark is a set of 16 diverse PCG environments that echoes the gameplay variety seen in the ALE benchmark Bellemare et al. (2015). The game levels, determined by a random seed,

Table 4: Measurements of compression efficiency $C(Z_C|O; \cdot)$ (Equation (9)) of the actor's representation ϕ_C in Procgen. Results highlighted in red when the auxiliary loss decreases the metric relative to the base algorithm, highlighted in green when the auxiliary loss increases the metric relative to the base algorithm, and highlighted in yellow otherwise. Auxiliary losses are applied to the actor (A) and critic (C) in the form of dynamics prediction (D), MICo, and advantage distillation (Adv).

Algorithm	$C(Z_C|O; V)$	$C(Z_C|O; L)$	$C((Z_C|O, Z'_C|O'; A))$
PPO	93.7 ± 3	88.4 ± 2	85.6 ± 4
PPO+MICo(C)	100.0 ± 0	90.3 ± 1	82.7 ± 3
PPO+MICo(A)	97.6 ± 2	92.4 ± 1	$\mathbf{64.4 \pm 6}$
PPO+D(A)	99.7 ± 0	90.2 ± 1	87.4 ± 3
PPO+D(C)	87.6 ± 4	$\mathbf{77.4 \pm 2}$	$\mathbf{99.1 \pm 0}$
PPO+D(A)+MICo(C)	91.0 ± 6	88.1 ± 2	84.4 ± 3
PPO+Adv(A)	96.7 ± 2	89.3 ± 1	87.6 ± 4
PPO+Adv(A)+MICo(C)	100.0 ± 0	89.9 ± 1	87.0 ± 3
PPO+Dr(A)	98.0 ± 1	90.0 ± 1	87.9 ± 3
PPO+Dr(C)	97.5 ± 1	87.0 ± 2	86.3 ± 3
PPG	99.2 ± 1	81.6 ± 2	90.3 ± 3
PPG+MICo(C)	93.0 ± 6	$\mathbf{90.9 \pm 2}$	91.8 ± 2
PPG+MICo(A)	100.0 ± 0	80.9 ± 2	84.4 ± 4
PPG+D(A)	100.0 ± 0	79.2 ± 2	91.3 ± 3
PPG+D(C)	$\mathbf{89.4 \pm 4}$	77.6 ± 2	$\mathbf{100.0 \pm 0}$
PPG+D(A)+MICo(C)	93.3 ± 4	$\mathbf{89.1 \pm 2}$	87.1 ± 4
PPG+Adv(A)	100.0 ± 0	80.9 ± 2	89.7 ± 3
PPG+Adv(A)+MICo(C)	99.9 ± 0	92.3 ± 1	93.1 ± 3
PPG+Dr(A)	98.7 ± 1	81.7 ± 2	90.2 ± 3
PPG+Dr(C)	96.4 ± 3	81.8 ± 2	85.8 ± 4
DCPG	99.5 ± 1	81.7 ± 2	92.1 ± 3
DCPG+MICo(C)	98.9 ± 1	$\mathbf{88.6 \pm 2}$	93.5 ± 2
DCPG+MICo(A)	99.8 ± 0	81.4 ± 2	87.2 ± 4
DCPG+D(A)	100.0 ± 0	80.7 ± 2	92.6 ± 3
DCPG+D(C)	$\mathbf{91.3 \pm 3}$	81.2 ± 1	$\mathbf{100.0 \pm 0}$
DCPG+D(A)+MICo(C)	99.6 ± 0	$\mathbf{87.4 \pm 2}$	92.7 ± 3
DCPG+Dr(A)	100.0 ± 0	81.3 ± 2	89.4 ± 3
DCPG+Dr(C)	97.0 ± 2	81.2 ± 2	90.7 ± 3

can differ in visual design, navigational structure, and the starting locations of entities. All Procgen environments use a common discrete 15-dimensional action space and generate $64 \times 64 \times 3$ RGB observations. A detailed description of each of the 16 environments is provided by Cobbe et al. (2020). RL algorithms such as PPO reveal significant differences between test and training performance in all games, making Procgen a valuable tool for evaluating generalisation performance.

We conduct our experiment on the easy setting of Procgen, which employs 200 training levels and a budget of 25M training steps, and evaluate the agent's scores on the training levels and on the full range of levels, excluding the training levels. We use the version of Procgen provided by EnvPool (Weng et al., 2022). Following prior work, (Raileanu et al., 2021; Jiang et al., 2021; Moon et al., 2022), for each game we normalise train/test scores by the mean train/test score achieved by PPO in that game.

For PPO, we base our implementation on the CleanRL PPO implementation (Huang et al., 2022), which reimplements the PPO agent from the original Procgen publication in JAX. We use the same

ResNet policy architecture and PPO hyperparameters (identical for all games) as Cobbe et al. (2020) and reported in Table 5.

We re-implement PPG and DCPG in JAX, based on the Pytorch implementations provided by Huang et al. (2022) and Moon et al. (2022). We use the default recommended hyperparameters for each algorithms, which are reported in Table 6. We note that our PPG implementation ends up outperforming the original implementation by about 10% on the test set, while our DCPG implementation underperforms test scores reported by Moon et al. (2022) by about 10%. We attribute this discrepancy to minor differences between the JAX and Pytorch libraries, and decided to not investigate further.

We conduct our experiments on A100 and RTX8000 Nvidia GPUs and 6 CPU cores. One seed for one game completes in 2 to 12 hours, depending on the GPU, algorithm, and whether the architecture is coupled or decoupled (for example, PPG decoupled can be expected to run 4x to 6x slower than PPO coupled).

C.3 BRAX

For our experiments in Brax, we implement a custom "video distractors" set of tasks, similar to those from (Stone et al., 2021). In this setup, a video plays in an overlay on the pixels the agent views. There is a disjoint set of videos between the training and testing environments. The random seed determines the environment's initial physics and the video overlay at the beginning of training. The pixels themselves are full-RGB $64 \times 64 \times 3$ arrays, but we use framestacking to bring each agent input to $64 \times 64 \times 9$ pixels.

Similar to the algorithms used in the Procgen experiments, we implement our algorithms in JAX and base them on ClearnRL.

We conduct our experiments on RTX A4500 Nvidia GPUs and 6 CPU cores. One seed completes in 7.5-48 hours, depending on the environment and its physics backend as well as the algorithm.

Table 5: Hyperparameters used for PPO in Procgen and Brax experiments. All runs employing a specific (or combination of) representation learning objective use the same hyperparameters.

Parameter	Procgen	Brax
PPO		
γ	0.999	0.999
λ_{GAE}	0.95	0.95
rollout length	256	128
minibatches per epoch	8	8
minibatch size	2048	512
J_π clip range	0.2	0.2
number of environments	64	32
Adam learning rate	5e-4	5e-4
Adam ϵ	1e-5	1e-8
max gradient norm	0.5	0.5
value clipping	no	no
return normalisation	yes	no
value loss coefficient	0.5	0.5
entropy coefficient	0.01	0.01
PPO (coupled)		
PPO epochs (actor and critic)	3	-
PPO (decoupled)		
Actor epochs	1	1
Critic epochs	9	1
MICo objective		
MICo coefficient	0.5	0.01
Target network update coefficient	0.005	0.05
Dynamics objective		
Dynamics loss coefficient	1.0	0.01
In-distribution transitions weighting	1.0	1.0
Out-of-distribution states weighting	1.0	1.0
Out-of-distribution actions weighting	0.5	0.5
Advantage distillation objective		
Advantage prediction coefficient	0.25	-

Table 6: Hyperparameters used for PPG and DCPG in Procgen experiments. Hyperparameters shared between methods are only reported if they change from the method above. All runs employing a specific (or combination of) representation learning objective use the same hyperparameters.

Parameter	Procgen
PPG	
γ	0.999
λ_{GAE}	0.95
rollout length	256
minibatches per epoch policy phase	8
minibatch size policy phase	2048
minibatches per epoch auxiliary phase	512
minibatch size auxiliary phase	1024
J_π clip range	0.2
number of environments	64
Adam learning rate	5e-4
Adam ϵ	1e-5
max gradient norm	0.5
value clipping	no
return normalisation	yes
value loss coefficient policy phase	0.5
value loss coefficient auxiliary phase	1.0
entropy coefficient	0.01
policy phase epochs	1
auxiliary phase epochs	6
number of policy phases per auxiliary phase	32
policy regularisation coefficient β_c	1.0
auxiliary value distillation coefficient	1.0
DCPG	
value loss coefficient policy phase	0.0
delayed value loss coefficient policy phase	1.0
MICo objective	
MICo coefficient	0.5
Target network update coefficient	0.005
Dynamics objective	
Dynamics loss coefficient	1.0
In-distribution transitions weighting	1.0
Out-of-distribution states weighting	1.0
Out-of-distribution actions weighting	0.5